

CrystEngComm

Accepted Manuscript



This is an *Accepted Manuscript*, which has been through the Royal Society of Chemistry peer review process and has been accepted for publication.

Accepted Manuscripts are published online shortly after acceptance, before technical editing, formatting and proof reading. Using this free service, authors can make their results available to the community, in citable form, before we publish the edited article. We will replace this *Accepted Manuscript* with the edited and formatted *Advance Article* as soon as it is available.

You can find more information about *Accepted Manuscripts* in the [Information for Authors](#).

Please note that technical editing may introduce minor changes to the text and/or graphics, which may alter content. The journal's standard [Terms & Conditions](#) and the [Ethical guidelines](#) still apply. In no event shall the Royal Society of Chemistry be held responsible for any errors or omissions in this *Accepted Manuscript* or any consequences arising from the use of any information it contains.

Recent advances in low temperature, solution processed morphology tailored ZnO nano-architecture for electron emission and photocatalysis applications

Soumen Maiti^{a*}, Shreyasi Pal^{a*} and Kalyan Kumar Chattopadhyay^{a#}

^aThin Films and Nanoscience Laboratory, Department of Physics, Jadavpur University,

[#]Corresponding Author E-mail: kalyan_chattopadhyay@yahoo.com

Abstract

Being beneficiary to several expedient features like low budget, straightforward processing, easy fabrication, large area deposition and physical flexibility association, low temperature solution processed electronic devices have gained traction in the eyes of the research community as difficulties involved with higher temperature conventional crystalline semiconductor devices are incrementally rendering them as passé. Over the last decade, amongst metal oxides, ZnO with rich genre of nano-forms has been documented as the candidature of highest economic impact by virtue of their diverse prosperity in the plethora of electronic and optoelectronic applications relying on the associated unique functional features like high mobility, excellent thermal stability and high transparency. To date, most of review articles in the literature were narrowed to ZnO nanostructures realized via vapour phase method whereas comprehensive study on solution processed nano-form and their widespread usage is still lacking. Current article mainly highlights an overview over recent development of multi-dimensional ZnO nano-architectures processed via low temperature, rational approaches and their functional properties in field emission devices and environment remediation. Additional to these portrayals on controlled morphology designing and usage perception, significant issues pertinent to such geometrical evolution and device performance determination and possible outlook for low temperature research on ZnO are also accounted.

Introduction

Metal oxide based semiconductors have lately emerged as a global hotspot of cutting-edge research owing to their propitious advantages in the devices of foreseeable future. Zinc oxide (ZnO), being a special candidate among them that possesses dual features of semiconductor and piezoelectric materials, has reinforced the rapidly intensifying nanotechnology arena through rich genre of nanomorphologies. ZnO, a direct wide band gap semiconductor (~3.3 eV) with a large electron-hole binding energy of 60 meV at room temperature, generally

exhibit thermodynamically stable hexagonal wurtzite structure.^{1,2} However, it also has other metastable cubic phases, namely high pressure rocksalt and zinc blende structures. Relying on several distinctive and fascinating features such as optical transparency, nontoxicity, electrochemical activities, chemical and photochemical stability, biocompatibility, high surface area, and embracing huge structural assortment etc., ZnO has already established its utility in fields such as electronic, optoelectronic, electrochemical, and electromechanical devices like solar cell, light emitting diode (LED), ultraviolet (UV) laser, field emission (FE) device, piezoelectric nano-generator etc.³⁻¹² Starting with zero dimensional (0-D) quantum dots or more general nanoparticles to one dimensional (1-D) nanowires, nanorods, nanospikes, etc.; two dimensional (2-D) nanoplates, nanosheets; three dimensional (3-D) nanoforms have been realized over the years via wide range synthesis protocols which can be categorised as electrospinning, vapour phase transport, chemical vapour deposition (CVD), metal-organic chemical vapour deposition (MOCVD), arc discharge, pulsed laser deposition (PLD), molecular beam epitaxy (MBE), flux method, sputtering, wet chemical and solution route etc.^{13,14} Among these protocols, vapour phase techniques, flux methods and other physical deposition procedures mostly require stringent criteria like high processing temperature, maintenance of high vacuum level, necessity of carrier gases, complex process controlling, and etc. In addition, usage of catalysts during experiment and their uncontrollable residue in the final product cast shadow over their universal applicability. Again, synthesis protocols like MBE, MOCVD suffer from low product yield and irregular deposition; PLD and sputtering methods lack reproducibility concern and electrospinning often produce polycrystalline nanoform.¹³ Furthermore, all these protocols have severe drawbacks as these are limited to specific substrates only. By circumventing all the aforesaid concerning issues, wet chemical synthesis route and solution phase synthesis have emerged as the apt alternative to realize ZnO nanoforms. Intriguing features like environment friendliness, low experimental budget, large area deposition over temperature sensitive substrate etc. made these protocols common practice for ZnO nanomaterials growth. In addition to the creative designing of ZnO nanomaterial via these wet chemical protocols, subtle morphology control to achieve device level performance from these nanoforms gained significant attention of researchers.

Several inclusive reviews on ZnO are already documented in the contemporary literature, however most of them illustrate the vapour phase produced artefacts and only very few discuss about solution processed nanoforms.^{13,14} Furthermore, previous reviews are

explicitly confined on 1D ZnO nanostructures, where the discussion on higher dimensional counterpart is still lacking. In this article, we have elaborately discussed low temperature solution processed starting from 0D to higher dimensional ZnO nanoforms. This entire article can be visualised in the following manner: the first section contains an overview on the morphological assortment realized through low temperature solution based synthesis protocol. In the next section, we discussed about the manipulations which are made for controlling and modifying its physical features like band gap engineering, conductivity alteration and etc. In the final and most decorative section, we illustrated the potential usage aspect of these nanoforms in field electron emission (FE), and photocatalysis. Not just regular survey of previous works, in this section we illuminated on the performance governing issues and their possible controlling also. Finally, a brief summary and discussion on the plausible ways out to circumvent the shortcomings and the other future scopes are made.

Growth of ZnO nanomaterials:

0D nanomaterial and nanoparticle:

Controlled precipitation, sol-gel, hydrothermal and solvothermal are the commonly adopted techniques for realization of ZnO nanoparticles at low temperature. Among these, controlled precipitation method generally yield nanoparticle with repeatable features. This protocol involves rapid and spontaneous reduction of zinc salt containing solution in the presence of a reducing agent, followed by the thermal treatment of the precipitation of ZnO precursor and then milling to remove the impurities. Frequent presence of high level of agglomeration in the final product is the demerit of this method. Reaction parameter like pH of the solution, processing temperature and etc. play pivotal role in this process. Simple as well as budgetary precipitation was used by Lanje et al.¹⁵ for the preparation of ZnO nanoparticle where they used zinc nitrate ($\text{Zn}(\text{NO}_3)_2$) and sodium hydroxide (NaOH). To minimize the agglomeration between the smaller particles starch was used which bind the nanoparticle surface in initial nucleation stage and prevented agglomeration. Using aqueous solution of zinc sulphate (ZnSO_4) and ammonium carbonate (NH_4HCO_3), Wang et al.¹⁶ have also made ZnO nanoparticle with nearly equal dimension where the particle size depended on reaction parameters. Recently, usage of surfactant in nanopowder synthesis becomes very common practice where they not only affected the growth, but also made huge impact on coagulation and fluctuation the particle.¹⁷ CTAB (cetyltrimethylammonium bromide) and sodium dodecyl

sulfate (SDS) are the frequently used surfactant. Li et al.¹⁸ have produced micron sized diverse shaped ZnO from the aqueous mixture of $\text{Zn}(\text{NO}_3)_2$ and NaOH in presence of SDS and triethanolamine.

Sol-gel method is other commonly adopted route for ZnO nanoparticle synthesis. Simplicity, repeatability, mild synthesis conditions and low expenditure are the hallmarks of this method. Further, surface modification of these nanoparticles with selected organic compounds results changes in their properties and widen their application range. Adopting sol-gel process, Benhebal et al.¹⁹ have prepared spherically shaped ZnO particle using zinc acetate, oxalic acid and ethanol. Ristic et al.²⁰ also obtained nanoparticle via sol-gel using a solution of tetramethylammonium hydroxide (TMAH), zinc 2-ethylhexanoate and propan-2-ol. TMAH, a strong base as compare to inorganic bases like NaOH creates high pH in the solution which ensures detoxification of nanoparticle with the cation of base.

Besides the afore-discussed synthesis protocols hydrothermal and solvothermal methods are also exercised for the realization of ZnO nanoparticles. Free from the usage of any organic solvent or necessity of any further processing of the products like grinding, calcination makes the hydrothermal technique simple and environmental benign. Additional advantages like low processing temperature, pressure dependent dimension controlling, high crystallinity and phase purity of the products upsurgers its appropriateness.^{21,22} Cheng et al.²³ have synthesised ZnO nanoparticle by hydrothermal technique using aqueous mixture of zinc chloride (ZnCl_2) and NaOH. Here, ZnCl_2 reacting with NaOH produces $\text{Zn}(\text{OH})_2$ which underwent for further processing in autoclave for appropriate times and produces nanoparticle. Experimental data suggested that with the increment in pH level, crystallinity and dimension of particle both upsurgers. Using $\text{Zn}(\text{OH})_2$ precipitation and thereby thermal processing it Ismail et al.²⁴ have also synthesized ZnO nanoparticle however the precipitation procedure is quite different from the previous. Reaction between $\text{Zn}(\text{CH}_3\text{COO})_2$, NaOH and hexamethylenetetramine (HMTA) resulted the precipitation. Here also the particles size was affected by the processing time, temperature and HMTA concentration. Impact of chemical synthesis on particle size and it's features was also determined by Musić et al.²⁵ Instead of regular hydrothermal procedures in laboratory oven several groups have also used microwave reactors during the hydrothermal.¹⁷ A detail comparison of ZnO nanoparticles prepared with different procedures of reaction stimulation was made by Choduba et al.,²⁶ where the supplied reaction energy sources were electric current, microwaves, Joule heating, heating of whole

autoclave and high voltage pulses. Among these, microwave and traditional autoclave synthesis produce the phase composition very near to pure ZnO whereas the other reactors shows impurity peaks along with ZnO. Using microwave reactors, zinc acetylacetonate and ZnO complex in several alkoxy-ethanol Schneider et al.²⁷ have prepared ZnO nanoparticles. They have found that the size and morphology of particles strongly depend on the precursor and achieved smallest particle using ZnO in methoxyethanol. In addition to hydrothermal, solvothermal technique is also chosen for the production of ZnO nanoparticle. Sphere shaped particles and hollow sphere was obtained via solvothermal method by Zhang et al.²⁸ Using solvothermal protocol Chen et al.²⁹ have also obtained ZnO particles which resulted from the reaction of zinc powder, trimethylamine N-oxide and 4-picoline N-oxide in presence of organic solvents and N,N,N',N'-tetramethylenediamine. Here, oxidising agent and the coordination ability of solvent played pivotal role in size determination of the nanoparticle.

1D ZnO nanostructure

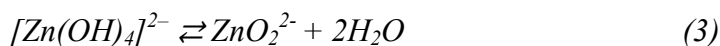
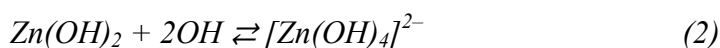
Basic growth mechanism of 1D ZnO nanoform

ZnO, an amphoteric oxide in nature having isoelectric point value ~ 9.5 usually crystallizes by the hydrolysis of zinc salt in basic conditions where the basic environment is achieved using strong or weak alkalis.¹³ Zn^{2+} ions, known to coordinate tetrahedrally can exist in a series of intermediates depending on the pH of the solution and temperature where the intermediary complexes after dehydration produces ZnO. In wurtzite ZnO, four most common face termination are Zn-terminated (0001) and O-terminated (000 $\bar{1}$) (c-axis oriented) polar faces and non-polar (11 $\bar{2}$ 0) and (01 $\bar{1}$ 0) (m-plane) surfaces. The non polar surfaces contain equal number of O and Zn ions while the polar surfaces are either O or Zn terminated. Two polar surfaces are highly significant from fundamental and technological point of view and possess slightly different physical and chemical properties. These polar surfaces and (1010) face are stable whereas, the non polar surface (11 $\bar{2}$ 0) is less stable face. Most often, the oppositely charged ions create negatively charged (000 $\bar{1}$) -O and positively charged (0001) -Zn polar surfaces, causing a normal dipole moment and spontaneous polarization along c-axis, together with a divergence in surface energy.³⁰ Such typical configuration results preferential adsorption of incoming precursors on the polar facets for the surface energy minimization of them during the ZnO nucleus formation. Further adsorption of monolayer of precursor transforms the polar surface into another polar one where the newly formed surface has

inverted polarity as compared to previous. This process continues over time and 1D morphology of ZnO evolved along the $\pm[0001]$ directions, bearing the non-polar $\{1100\}$ and $\{2110\}$ side facets to the solution.¹³

Growth in general basic solutions

General incapability of the divalent metal to hydrolyze in acidic condition necessitates the presence of alkali solution for the growth of ZnO nanostructures where KOH and NaOH are the mostly used alkali compounds. However, amongst these two KOH assisted ZnO growth is more preferable one as probability of incorporation of KOH in ZnO is very low as compared to NaOH due to the larger ionic radius of K^+ . Additionally the attraction to the Na^+ by the OH^- creates a virtual capping around the nano-crystal and hindered the further growth. The main reaction procedures going behind such sort of growth in general alkaline solution is presented below:^[13, 31]



As the nucleophilicity of the OH^- ion is higher than H_2O , in this type of aqueous synthesis, the coordination spheres around the central Zn^{2+} ion are predominated by hydroxyl ions. The growth process commences with the co-ordination Zn^{2+} and OH^- following which the coordinated complex goes through dehydration via proton transfer and produces aggregate in the form of $[Zn_x(OH)_y]^{(2x-y)+}$ having octahedral symmetry.¹³ Consideration of Bronsted acidity of the aqueous complexes is important to recognize some intriguing consequences. For any polyprotic acid (or conjugate of a base) it is possible to sketch a distribution diagram based on all the operative hydrolysis constants. In concentrated hydroxide solutions, Zn^{2+} forms anionic species (ZnO_2^{2-}) which are the conjugate bases of the oxide or hydroxide. These ionic species are soluble in water, at least to a certain extent, while most neutral species precipitate. Though the above mentioned equations suggest only formation of $Zn(OH)_4^{2-}$ as growth intermediate however the product form can differ depending upon the parameters like pH value of the solution and Zn ion concentration in it. At the start, these aggregates comprise of nearly 50 ions which mature quickly to 150 ions and wurtzite form ZnO domains nucleated at central region. This central core is composed of Zn^{2+} and O^{2-} only, slightly different to surface of the aggregate where still large number of OH^- are present along with Zn^{2+} . Increasing in

size further to over 200 ions by connotation and dehydration of Zn^{2+} and OH^- ions nanometric wurtzite core formed.^[13]

In such type of growth pH value of the aqueous solutions decides the crystal phase of deposits. Both ZnO and $\text{Zn}(\text{OH})_2$ are thermodynamically stable within the pH range of 7-14 at a 0.01 M Zn concentration.^[31] At pH value >9 , soluble Zn (II) species in the form of $\text{Zn}(\text{OH})_2$, $\text{Zn}(\text{OH})_4^{2-}$ and etc. increase in the solution and with higher chemical potential of OH^- ion the reaction is expected to move forward. Owing to such rise in precursors concentration and chemical potential of OH^- with increasing pH, formation of ZnO at pH >9.0 occurs.^[31] It is very worthwhile to mention here that OH^- in solution has also a significant effect on the nature of growth interface, especially on polar faces and thereby on the rate incorporation of growth unit on these.^[32]

Besides $\text{Zn}(\text{OH})_4^{2-}$, ZnOOH^- and ZnO_2^{2-} are the other two main Zn species in hydrothermal alkaline solution where the prevalence of specific one depends on the concentration of OH^- and temperature of the solution.^[33] With increasing concentration of the OH^- ion $[\text{ZnO}_2^{2-}]$ -species also enhances in growth solution, predominance of which in initial is responsible for the polar growth. The outmost layer of the (0001) and (000 $\bar{1}$) faces comprise of Zn^{2+} and O^{2-} ions respectively. As the growth process on this Zn terminated surface involves reaction between unlike-charged entities thus rate of reaction should be much higher than that same on O terminated surfaces.^[34]

Instead of water, growth of ZnO nanostructures can also be possible using several other solvents ranging from organic like ethanol, methanol to ionic liquids which confirms that O_2^- comes from solvents not the alkali. Though the aforesaid reaction processes seem very simple however in reality it is very complex. Oxygen molecules (O_2) that have not been considered in the equations play a pivotal role. For instance, dissolved O_2 molecules in the solution have a significant impact over the crystallinity in the final production.^{13,35}

It is well established that the morphology of the polar inorganic crystal strongly depends on the crystal-solvent interfacial interactions.³⁶ ZnO, being a polar material, is strongly influenced by the saturated vapour pressure and polarity of the solvents during growth. Directed by the growth rate differences of polar and non-polar surfaces in different solvents of varying polarity, nanowires with different dimensions were resulted. Polar surfaces of ZnO, via making strong interaction with the polar solvent, hinder the precursor molecule adsorption. Not only polar, 1D nanostructure was also synthesized in non-polar solvent

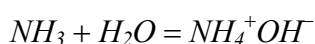
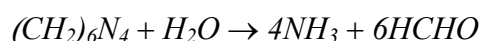
also.³⁷ Growth of 1D ZnO nanostructure in alkaline solutions not confined to bulk synthesis only, such common solution routes are also adopted for the realization of thin film. Wu et al.³⁸ have demonstrated highly oriented ZnO 1D nanostructure arrays on the zinc foil at nearly room temperature using $\text{Zn}(\text{NO}_3)_2$ and KOH. Direct oxidation of zinc foil in alkaline zincate ion solution at low temperature ensued nanoneedles whereas slight elevation in temperature resulted nanorods array. In its place of zinc foil, Li et al.³⁹ have synthesized ZnO nanorod arrays on ZnO seeded Si substrate and controlled the density and dimension of nanorods via adjusting the molar ratio of $\text{Zn}(\text{NO}_3)_2$ to NaOH. Recently our group³⁶ has demonstrated ZnO nanostructures with different morphology via one pot ambient conditioned approach where the nanoforms were spontaneously formed over zinc foil in alkaline supersaturated solution containing zinc salt. Shape of nanostructure, a key issue for practical usage, was tailored by only manipulating the counter anion of zinc salt used.⁴⁰ Figure 1(a-d) shows the zinc counter ion varied morphological assortment.⁴⁰ Beyond seeded substrate and zinc foil we have also prepared large scale arrays of ZnO nanospikes with ultra-sharp tips on heterogeneous substrates at ambient condition through a KOH assisted novel wet chemical route.⁴¹ The deposition technique is a general one in the sense that it is compatible with complex substrates and independent of the nature of substrate. Liquid phase activation of the substrates with KMnO_4 lead $\text{Mn}(\text{O})\text{OH}$ seed formation over it which served as low energy nucleation site for heterogeneous growth. Depending on the substrate pre-treatment, arrangement of nanospikes over substrates was also changed from densely packed nanoflower to distributed one.

Ammonia and Hexamethylenetetramine (HMTA) assisted growth

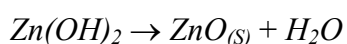
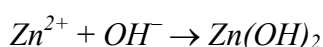
Not only KOH and NaOH can create alkali environment for ZnO growth, weak bases like ammonia solution and other amines like HMTA are also capable of doing the same. Growth of ZnO nanowires in the NH_3 , H_2O environment was elaborately studied by Liu et al.⁴² They have reported vertically aligned ZnO 1D nanostructures on conducting alloy substrate in mild solutions at low temperature in the absence of any seeds, catalysts, and surfactants. NH_3 , H_2O not only creates basic atmosphere for ZnO growth, it also facilitates the heterogeneous nucleation.^{43,44} It was experimentally verified that gradual decrement of Zn^{2+} ions slowed down the nanostructure growth with time and after long reaction span it arrived at growth-dissolution equilibrium.¹³ Such bottleneck can be bypassed by several ways among which

further addition of zinc salt and ammonia in the solution or restocking of growth solution are the mostly adopted routes.

Besides general alkalis, mostly used amine for ZnO synthesis is HMTA which is a non-ionic cyclic tertiary amine. Though the exact function of HMTA in ZnO growth is still undefined however recent study suggest their role as a bidentate Lewis base which coordinate and bridge the Zn^{2+} ions.¹³ The most commonly adopted route for ZnO 1D structure is $Zn(NO_3)_2$ and HMTA assisted hydrothermal synthesis where the nitrate salt provides Zn^{2+} and water molecules in the solution delivers O_2^- ions for ZnO growth. Besides the coordination and bridging up of Zn^{2+} ions in ZnO, HMTA has several roles to play like weak base, pH buffer and growth rate control of ZnO. Intrinsic growth habit of ZnO along the direction of polar surfaces is facilitated by the preferential attachment of HMTA on the non-polar facets.^{45,46} Hexamine, a rigid molecules at elevated temperature mingling with water produces ammonia which further by reacting with water decompose to hydroxide ion (OH^-) and forms $[Zn(NH_3)_4]^{2+}$ separately.^{13,47}



Rate of hydrolysis of HMTA in water is very critical factor in this sort of synthesis where the quick one has arrested ZnO growth after some times. Rapid hydrolysis of HMTA produces OH^- very quickly which create a basic environment. Such alkaline environment prompt the precipitation of Zn^{2+} ions in solution and rapid consumption of the nutrient thereby hinders the growth.⁴⁸ Further, decomposition of $Zn(OH)_2$ following the underlying equation, produce ZnO at higher temperature where the temperature elevation could be attained using oven,⁴⁹ under ultrasonication,⁵⁰ in microwave,⁵¹ and even by sunlight.⁵²



Abovementioned reaction pathways depicted in hexamine assisted growth procedure are in equilibrium, which can be altered in forward or backward by adjusting the reaction parameters. In general, morphology and aspect ratio of ZnO nanowire are determined by the growth duration and processing temperature whereas the number density of nanowire is governed by the nutrient concentration. The reaction process commence very slowly at room temperature,¹³ however application of microwave heating speeds up the reaction rate.⁵¹ Besides the nitrate salt, salts containing other counter ions are also capable to produce ZnO nanostructures where the nanostructures' morphology are determined by the choice of

counter ions. Besides the Zn counter-ion, factors like complexing ligand, choice of amines also control the morphology of the ZnO nanoform.

Most important aspect of ammonia and amine assisted growth lays in the realization of ZnO 1D nanostructure over seeded substrate. Using ZnO seed layer and adopting these low temperature wet chemical route, ZnO nanostructure was realized on wide range substrates like silicon (Si), glass/ITO coated glass, paper, polyethylene terephthalate (PET), thermoplastic polyurethanes, carbon fibers and few are displayed in Figure 2(a-m).^{42,49,53-61} Adhesion of seed with substrate is a critical parameter for nanostructure growth can be improved via introduction of a metallic layer over the inorganic substrate and incorporating a interfacial bonding layer on polymer substrate.^{13,62,63} Seed layer over the substrate can be prepared via sputtering, spin coating a ZnO sol or colloidal solution of quantum dots. Growth of ZnO nanowire starts with nucleation over the seed layers. More precisely, the nanowires preferentially nucleate from the cup tip near the grain boundary between two ZnO grains in the seed layer.⁶⁴ Diameter of the outgrowing nanowires largely influenced by the texture, thickness and grain size of the underlying polycrystalline seeds. Ji et al.⁶⁵ have reported the increment in nanowires average diameter and decrement in their number density as the consequence of thickness enhancement of seed layer. Despite of being random in plane alignment of ZnO seed c-axis generally remain perpendicular to substrate however there were few reports of non-perfect c-axis orientation also.¹³ Not only the diameter, vertical alignment of nanowires also dictated by the crystallinity of the underlying seed layer. A simple seeding method for producing vertical ZnO nanowire arrays on any flat substrate that can survive heat treatments at 200 °C was presented by Green et al.⁶⁶ Besides the pre-synthesized seed layer on arbitrary substrate metallic Zn foil also solve the purpose of both seed and substrate. Zn foil in open air or in solution very easily transforms to ZnO. Using an aqueous mixture of ammonia and alcohol Fang et al.⁵⁴ have realized ultrathin ZnO nano-fibres in a dense array over Zn foil via hydrothermal technique. In a slightly modified protocol, Yang et al.⁶⁷ have synthesised large-scale highly oriented ZnO nanorod arrays on Zn foil by simple hydrothermal reaction using simple aqueous ammonia.

Patterned growth of ZnO

To achieve devices level performances from the synthesized nanoforms its arrangement over the substrate via site selective, density and orientation controlled growth become an area of research. Such defining controlled over the nanostructure growth on substrate is generally

accomplished via lithography. These lithographic techniques may be varied from simple photolithography to complex electron beam lithography, interference lithography and etc. Photolithography is the technique that involves UV light assisted transfer of pattern from mask to photosensitive material on substrate. Combining photolithography and low temperature aqueous method patterned growth of ZnO nanorod on Si substrates was demonstrated by Kang et al.⁶⁸ Similar combinational recipe was adopted to prepare patterned ZnO nanorod by Tak et al.⁴³ Compare to photolithography, electron beam lithography (EBL) gives more high resolution pattern. Bottlenecks involve in photolithography arise due to diffraction limit of UV light is bypassed by the accelerated electrons with very small wavelength. In EBL, commonly used growth masks are inert material like SiO₂ or polymer resist like polymethyl methacrylate (PMMA).¹³ Besides the benefits, this protocol has few demerits also like high experimental cost, low throughput and etc. Going beyond conventional ZnO seed layer assisted growth; Weintraub et al.⁶⁹ have reported a wet chemical protocol for site-selective growth of individual ZnO nanorods in patterned arrays on organic substrates. In this work, EBL using a PMMA mask on a Kapton polyimide substrate with an Au intermediate layer was employed to define nanorod positions. By combining the EBL and hydrothermal method ZnO nanowire arrays with high degree control over size, orientation, dimensionality, uniformity was achieved on general inorganic substrates in absence any catalyst.⁵⁷ Addition to these two, several other lithographic techniques also like nano-sphere lithography, laser lithography, and interference lithography adopted to realize ZnO on pattern substrate. Nanosphere lithography been proven to be a flexible and budgetary technique for the pattern of nanostructure with long-range periodicity where a monolayer colloidal crystal (MCC) used as mask. Simplicity, cost effectiveness and high throughput are the highpoints of the technique. Patterned arrays of ZnO nano-pillars with controlled morphology and orientation were fabricated by Li et al.⁷⁰ directly on Zn foils via wet chemical route with the aid of MCC. Laser interference lithography is other way to achieve ultimate resolution for a certain wavelength without requiring complex and high numerical aperture optics. Practically unlimited depth of focus and large exposure fields are the advantages of this technique.⁷¹ Patterning of surfaces with Zn using the laser induced forward transfer (LIFT) technique and subsequent chemical growth of ZnO thin films was realized by Claeysens et al.⁷² Figure 3 (a-g) illustrates several ZnO nanorod arrays grown selectively on pre-patterned substrate using lithographic techniques.^{68-71,73,74} These ZnO nanoforms on patterned substrates showed enormous propitious in electronic and optoelectronic devices.

Electrodeposition

Electrochemical deposition (ECD) is soft chemical method and powerful practice to achieve uniform and large area nanostructure at atmospheric pressure and at low temperature. ECD by adding an external driving enables the reactions which are non-spontaneous otherwise. This protocol is very attractive one due to its low experimental budget and can be performed on various substrates including rigid planar, cylindrical, flexible and complex substrates. Moreover, this is an effective protocol for the doping of ZnO nanostructures. Usually a three electrode system is used for electrodeposition where the standard Ag/AgCl electrode acts a reference, Pt electrode as counter. Electrical bias through the system is maintained by a voltage or current source to maintain constant driving force.¹³ Direct ECD of ZnO films was primarily performed by Peulon et al.⁷⁵ In the same year, Izaki et al.⁷⁶ have also deposited ZnO films on conductive glasses from a aqueous Zn(NO₃)₂ electrolyte kept at 335K. Perhaps the commonly used zinc source for this type of synthesis is ZnCl₂. Using ZnCl₂ and potassium chloride (KCl) mixture solution as electrolyte, aligned ZnO nanowire over glass substrate was realized by Konenkamp et al.⁷⁷ During the reaction, O₂ gas was constantly bubbled into the solution and reduction of which at cathode produced OH⁻. These not only increased the pH value also by co-ordinating with Zn²⁺ formed ZnO.¹³ Irrespective of zinc salt used, the ratio between the OH⁻ generation rate and the Zn²⁺ diffusion rate was considered as the pivotal parameter for ZnO nanowires synthesis in this method. Elias et al.⁷⁸ have found that ZnCl₂ concentration is an important parameter for the dimension controlling of ZnO nanowires. It is well accepted that Cl⁻ has a preferential adsorption tendency where it presumably binds the Zn²⁺ terminated surfaces and by hindering the growth along (0001) plane triggered formation of 2D nanoform. Xu et al.⁷⁹ have prepared ZnO nanostructures by controlling the growth rates of various facets using suitable capping agents. Changing the compositions of capping agents they obtained different morphology like hexagonal nano-tapers, hexagonal platelets and etc. Apart from ZnCl₂, KCl also plays a significant role on the electrodeposition of ZnO nanowire.⁸⁰ Besides its role as a supporting electrolyte, its concentration in the solution also played vital role. Increase in KCl concentration resulted in augmentation of the ZnO deposition efficiency while low concentration made an impact on lattice parameter. By changing the Zn²⁺ precursor and supporting electrolyte several groups have also prepared ZnO nanostructures. Elias et al.⁸¹ has reported electrodeposition of ZnO nanowire arrays from the reduction of dissolved molecular O₂ in solutions containing

different anions. Nanowires exhibiting the highest and lowest aspect ratios were obtained in acetate and chloride solutions respectively. Besides regular electrodeposition, direct template electrodeposition techniques were also adopted for ZnO nanostructures synthesis⁸² however removal of the template after the growth associated with these protocols is a serious drawback.

Besides regular nanorod and nanowire like 1D nanoform, several other 1D nanostructures also synthesized using low temperature solution route. ZnO nanobelt is peculiar 1D nanoform which was mostly achieved via vapor phase protocol. Using hydrothermal process Xi et al.⁸³ have prepared ZnO nanobelts with lengths of 10–20 μm and widths of 50–500 nm. Similar sort of nanobelt structure on Zn substrate was also achieved by electrochemical route.⁸⁴ Besides nanobelt, tubular ZnO is another cultured 1D nanoform which have several usage potential due to their peculiar structural novelty. ZnO nanotube or ring like nanoforms was achieved by several ways like ultrasonic pretreatment of reaction system,⁸⁵ template wetting process,⁸⁶ hydrothermal route,⁸⁷ two-step etching,⁸⁸ and etc.

Higher dimensional nanostructures:

Not being restricted to 0D or 1D, higher dimensional nanostructures like 2D, 3D and nanostructures with more geometrical intricacy was also explored in order to achieve more interesting and intriguing features. Higher dimensional nanoforms possessing large specific surface area are beneficial for various applications. However, realization of them especially in 2D is very difficult as ZnO has inherent tendency of growing in 1D, resulted from the highest growth velocity along c-axis. Capping off the positive Zn terminated (002) surface with appropriate anions could be the one possible way to restrict the 1D growth. Using citrate ion as growth hindering agent of (002) plane, Tian et al.⁸⁹ have synthesized 2D nanoplate and their assembly. Illy et al.⁹⁰ have grown ZnO films on polycrystalline Zn foil by cathodic electrodeposition, where the alteration in reaction parameters result the variation in morphology from 1D nanorod to 2D nanoplate and finally to 3D crystal. Using similar electrodeposition technique, 2D ZnO nanowall on ITO glass substrate was prepared by Pradhan et al.⁹¹ In another work, they have also demonstrated growth of both 1D (nanopillar) and 2D (nanowall) nanoform on In_2O_3 -coated PET substrates using electrodeposition.⁹² XPS depth-profiling study showed the presence of Cl^- ions throughout the nanostructure which further validated the role of Cl^- ions as capping agent for the (0001) plane in the formation mechanism of nanowall. Besides electrodeposition, hydrothermal and sonochemical approach

was also adopted for the realization of 2D ZnO nanostructure.⁹³ Besides the common 1D and 2D nanoform array, assembly and integration of low dimensional building block into 3D hierarchical superstructures are of paramount interest. Coalescing of 1D nanoform via sequential nucleation and growth in one unit is the commonly used pathway to realize hierarchical at low temperature. Zhang et al.⁹⁴ have reported site-specific sequential nucleation and growth route for systematic building of hierarchical, complex and oriented ZnO micro/nanoform in solution synthesis. Using similar nucleation and growth protocol brush like hierarchical ZnO nanostructures assembled from initial 1D ZnO nanostructures were prepared hydrothermally by Zhang et al.⁹⁵ Via a simple selective hierarchical growth sequence Ko et al.⁵⁵ have also produced nanoforest of high density, long branched tree-like multigeneration hierarchical crystalline ZnO nanowire. Following successive nucleation and growth of branched ZnO nanowires on conductive glass substrates have also fabricated by Cheng et al.⁹⁶ Besides sequential nucleation and growth, self-assembly of lower dimensional nanoform is another way. Self-assembly of hierarchical ZnO superstructures by low-temperature chemical bath deposition method was reported by Pachauri et al.,⁹⁷ where subtle control over reaction kinetics produced flower-like, rolling-pin-like, viscous-fingers-like and antenna-like diverse nanoforms. Going beyond inevitable amine assisted route, surfactant based growth protocols were also explored. Flower-like ZnO nanostructures consisted with sword-like ZnO nanorods, have been prepared by CTAB assisted hydrothermal process at low temperature. Not only surfactants, with proper choice of solvent higher dimensional nanoforms were also realized. Using ethylene glycol (EG) as solvent 3D ZnO hollow micro-hemispheres consisting of several 1D nanorods was also synthesized via solvothermal procedure⁹⁸ where EG and solvothermal process played the critical role in the formation of 3D ZnO hollow micro-hemispheres. Besides these nanoforms, very exciting urchin like ZnO microsphere composed of 1D nanoneedle were also prepared by thermal processing of hydrozincite synthesized via homogeneous precipitation of $Zn(NO_3)_2$ and urea in presence of non-ionic surfactant polyethylene glycol.⁹⁹ Not only 1D assembly, 3D architecture composed of 2D building block also reported in the literature. Nestlike 3D ZnO porous structures have been synthesized through annealing the zinc hydroxide carbonate precursor, which was resulted from the hydrothermal process with the aid of glycine, Na_2SO_4 , and polyvinyl pyrrolidone.¹⁰⁰ Utilizing dodecyl benzene sulfonate as structure-directing agent hierarchical ZnO nanoform made of 2D nanodisk were also synthesized. Downshifting the processing temperature further to room temperature Wang et al.¹⁰¹ have demonstrated 3D ZnO

mesocrystals constructed with 2D sheet subunits using complexing agent NH_4F . Sonochemistry based facile approach for ZnO nanosheet-based 3D hierarchical nanoform with multiple functions was also reported in literature.¹⁰² Further there are many reports on the pairing of 1&2D nanostructure in to 3D assemblies also.¹⁰³ With proper choice of starting materials scientist also achieved numerous novel morphology such as pagoda shaped nanoform,¹⁰⁴ coral reef-like ZnO,¹⁰⁵ cauliflower-like ZnO, dandelion-like ZnO and etc.¹⁰⁶ A pictorial presentation of few hierarchical ZnO nanoforms comprising of low dimensional building block is illustrated in Figure 4.^{85,94,100,104,106-119}

Heterostructures:

Driven by the compulsion to explore manifold functionalities via uniting the physical aspects of several materials, modern edge research has witnessed colossal interest regarding fabrication of heterostructures. Not only performance enhancement, generation of novel interface phenomenon was also attained by realizing ZnO based heterostructure. FESEM images of some ZnO based heterostructures with intriguing geometry are shown Figure 5(a-l).^{59,154-164} Hierarchical ZnO poised with ultrathin nanosheets were fabricated through hydrothermal method and CdS particle were incorporated on wurtzite ZnO sheets with the assistance of ultrasonic irradiation.¹⁵⁷ Like CdS, several narrow bandgap semiconductors like CdSe and CdTe, have also attached where such modification have improved the overall energy conversion efficiency in photovoltaic.^{165,166} Besides these semiconductors, several metal oxides were also attached with ZnO. Cuprous oxide (Cu_2O) and cupric oxide (CuO) both attached with ZnO for different purpose. ZnO nanorods were grown hierarchically on Cu_2O nanoneedles to form a $\text{Cu}_2\text{O}/\text{ZnO}$ hetero-nanobrush assembly.¹⁶⁰ Such decoration have increased the overall aspect ratio which in turn resulted a boost in field emission performance. Recently we have fabricated an oxide based nanostructure hybrid by integrating low bandgap CuO nanosheet with high bandgap 1D ZnO nanowires on flexible and rigid substrate both which exhibited excellent photocatalytic activity.¹⁵⁶ CuO/ZnO heterostructure produced via photochemical deposition of CuO on hydrothermally grown ZnO nanorods exhibited stable gas response, reversibility and enhanced H_2S gas responses compared to pure ZnO nanorods.¹⁶⁷ SnO_2 , a wide band gap n type semiconductor shows the similar crystal growth habit as ZnO in aqueous media. Due to this, several heterostructures comprising ZnO- SnO_2 were documented. Li et al.¹⁵⁴ has reported glucose-assisted hydrothermal process for the design of complex and functional ZnO/ SnO_2 nanostructures where glucose molecules

mediate the growth heterostructure by interaction between the Zn/Sn elements and hydroxyl groups in glucose molecule. Similar combinational heterostructure was also achieved by Wang et al.¹⁶⁸ Cerium oxide (CeO_2), one highly active oxide catalysts in rare earth oxide series shows great potential in photocatalysis. Uniting CeO_2 with ZnO few heterostructures realized for functionality improvement.^{164,169} Combing other oxides like TiO_2 , NiO, MnO_2 etc. numerous heterostructure were also synthesized.^{162,170,171} Aside to metal oxide researchers have attached sulfides materials with ZnO. Via two-step solution protocol CuS/ZnO heterostructure was fabricated on mesh substrate which exhibited superior photocatalytic activity compared to bare ZnO.¹⁷² ZnO/PbS core/shell were also realized where ZnO nanowires were firstly fabricated and then the synthesis of ZnO/ZnS and ZnO/PbS core/shell nanowire arrays were realized by a chemical conversion method.¹⁷³ ZnO/ZnS core/shell was also prepared by immersing ZnO nanorods in Na_2S and nitrate hexahydrate solution alternately.¹⁷⁴ Via combining carbonaceous materials like graphene, carbon nanotube (CNT) with ZnO several functionality improvements were achieved by the researchers. With the expectation of achieving better field enhancement, we have attached reduced graphene oxide with ZnO and obtained high field emission from the hybrid.¹⁵⁵ Bu et al.¹⁷⁵ have also prepared graphene–ZnO composite where the graphene coating significantly improves the photocatalytic property of the combinational. Besides graphene, Zhang et al. have prepared ZnO-CNT heterostructure via hydrothermal route.¹⁷⁶ ZnO nanowires were grown on modified well-aligned carbon nanotube (CNT) arrays where the pre-deposited ZnO grains on the CNTs served as the nucleation sites for the growth of ZnO nanowires. Apart from these above stated heterostructure ZnO and noble metal based hybrid were also documented in the literature. Fan et al.¹⁷⁷ have synthesized Ag–ZnO heterostructures in which ZnO nanorods were selectively grown on single-crystalline Ag nanocubes. Another noble metal, Au was decorated homogeneously on the surface of ZnO nanorods by He et al. where nanoparticles have good interfacial connection and strong binding with ZnO nanorods.¹⁵⁹ Using chemically driven self-assembly method Pt nanoparticles were also introduced on the surface of ZnO nanowires.¹⁷⁸

Doping of ZnO:

Doping with foreign element is the most common practice to control the physical features like conductivity type, electrical conductivity, and band gap of semiconductor. Both types of doping i.e. n-type and p-type were made in ZnO nanoform. In general, undoped ZnO exhibit n-type conductivity with electron concentration as high as 10^{21} cm^{-3} ,¹⁷⁹ where the n type

behavior is due to presence of the native defects like zinc interstitials and oxygen vacancy. Mobility of electron in undoped ZnO is not constant and it greatly depends on preparation method. Cui et al.¹⁸⁰ have doped ZnO nanowires with Cl using the mixture solution of $\text{Zn}(\text{NO}_3)_2$, $6\text{H}_2\text{O}$, HMTA and ammonium chloride (NH_4Cl). Successful chlorine doping not only lead modification in nanowire dimension it also reduced the amount of oxygen defect in them. Close inspection of the observed photoluminescence (PL) spectra suggested blue-shift of the band-edge emission peak, an indication of bandgap widening with the increase in Cl doping percentage. Besides Cl, Aluminum (Al) doping was also documented in literature. Fang et al.¹⁸¹ have explored the effect of Al doping on mechanical, piezoelectric, and semiconductive properties of ZnO nanorods. Majumder et al.¹⁸² also successfully doped Al within ZnO and have achieved Al doped transparent ZnO thin films using a chemical technique. Though the doping did not change in band gap significantly however it resulted a huge change in resistivity of the sample. Prior to doping resistivity of sample was $3.8 \Omega \text{ cm}$ which decreased and remained in the range of $0.27\text{--}0.32 \Omega \text{ cm}$ for up to 4 % Al doping. Aside Al, other group V elements were also doped in ZnO. Following hydrothermal route Cimitan et al.¹⁸³ have realized Indium (In) and gallium (Ga) doped ZnO nanoparticles. Compare with the number of n-type doping, works on p-type doping is still lacking. p-type doping was mostly achieved in vapor phase and stability and reproducibility of such p-type conductivity is still remained a questionable issue. To attain successful p-type doping group I or group V elements should be incorporated to replace the zinc or oxygen atoms in ZnO. Hsu et al.¹⁸⁴ have demonstrated a versatile method for the growth of p-type or n-type ZnO nanorods from the same growth solution at low temperature where the preparation of seed layer for nanorod growth played the vital role in conductivity control. ZnO fabricated with zinc acetate derived seed layers exhibited p-type characteristics whereas the same fabricated over electrodeposited seed showed n-type behavior. Further huge amount of work is also done on transition metal doping. Li et al.¹⁸⁵ have hydrothermally produced ZnO nanorods doped with Mn, Cr and Co. Results suggested that dopant assimilation was in good agreement with solution concentration in case of Mn and Co, while for Cr dopant the incorporation was low. For all three dopants, the observed morphology was different from undoped ZnO. ECD is a powerful technique for the doping of ZnO. Using ECD Cui et al. have prepared Co and Ni doped ZnO nanowire and observed anisotropic ferromagnetism with an easy direction of magnetization either perpendicular or parallel to the wire axis Ni-doped ZnO nanowires at room temperature.¹⁸⁶

Applications of low temperature solution processed ZnO nanostructures:

ZnO with their broad range of nano-morphologies relying on their fascinating chemical and physical features have found their usage potential as UV detector, gas sensor, solar cells, photocatalyst, field electron emitter and etc. From this widespread usability, in this article we will discuss elaborately on their potential as electron field emitter, photocatalyst and on performance determining issues related to them.

Field emission:

To escape from metal, electrons have to overcome the potential energy barrier at the surface. Gain in energy to overcome the barrier can be accomplished by various energy sources such as heat, light or electricity etc. Among which, the phenomenon of electric field assisted electron emission from the surface of a condensed phase (metal or semiconductor) into other phase (vacuum), generally known as field emission (FE) or cold cathode emission, have several benefits over the other electron emission process such as relatively insensitive to ionizing radiation and temperature variations etc. Furthermore, high electron emission efficiency compare to other procedures make it significant for device application compared with other procedures. Field emission phenomena can effectively be summarized as the weakening of the vacuum barriers in close proximity of a solid surface as a consequence of local perturbation of applied field produced by atomic level surface undulations, which ultimately manifests as an increased in the electron tunnelling probability. At low temperature for a metal, the FE process can be easily understood through the illustration of figure 6a. Under the application of strong field, the potential barrier in the vicinity of metal is distorted along the line AB (or AC) and takes a triangular shape through which electrons can tunnel easily. With further thinning of the potential barrier electron tunnelling increases i.e. more number of electrons tunnel efficiently from the metal into vacuum. Most of the prior documentations on field emission has predominantly confined with planar cathode where the applied electric field dropped linearly. However with the advent of semiconductor nanostructures research on this regard has been intensified as the unique geometrical features associated with them facilitates the deformation of the electric field by greater extent and thereby resulting in a curvilinear drop across the vacuum gap which further eases the electron tunnelling phenomena. Nanostructure based cold cathodes had already established their usage prospective in modern electronic devices. In this regard, CNT has taken their supremacy in the frontier research due to offering high emission current at low operating voltage. But the

stringent criteria involved in their synthesis process, instability in harsh situation, and etc. motivate researchers for the realization of suitable alternatives. Among the most cultivated materials, nanostructured ZnO with their broad structural diversity have grabbed a significant attention owing to the facile realization of nanoarchitecture. Also being an oxide material, the degradation probability in emission performances by residual gases is also minimizing in ZnO. Figure 6b shows schematic of a FE measurement setup where ZnO nanostructure over conducting substrate or the powder sample on conducting tape over a flat steel plate acting as cathode while another stainless steel electrode solves the purpose of the anode. FE measurements are always carried out in high vacuum to nullify the impact of residual gas molecules. Zhang et al.¹⁸⁷ suggested that a typical pressure $\sim 10^{-7}$ Pa leads a mean free path $\sim 1 \times 10^4$ m of the molecules which is very much higher than the cathode-anode separation. Thus the contribution from the molecules between the ambient and the electrodes can be ignored. Lowering the vacuum condition from this level increases the collision probability with the gas molecules and below ($>10^{-4}$ Pa) such emission behaviour might not be feasible. FE, a quantum mechanical phenomenon can also be coined as Fowler–Nordheim (FN) tunnelling strongly depends on several parameters like emitting materials intrinsic features such as conductivity, work function, shape and morphology of the cathode, inter emitter separation thereby field screening among themselves, presence of defect and geometry of the underlying substrate and etc. The FN formalism is generally used in order to quantitatively describe the FE process and according to which FE current density (J) is related with the applied field (E) as follows, $J = (A\beta^2 E^2 / \phi) \exp(-B\phi^{3/2} / \beta E)$ Where A and B are constants, $E = V/d$ (d is the anode-emitter distance), ϕ is the work function of the emitter and β is the geometrical field enhancement factor which designates the amplification ability of the emitter to intensify the applied electric field at the emitting site. From the slope of the graph of $\ln(J/E^2)$ versus $1/E$, FN plot β value can be estimate for known work function value. Generally for the quantitative analysis of FE results the considered ϕ value is 5.3 eV for ZnO.^{40,41} In next section we will discuss the recent development on solution processed ZnO nanoform based field emitter and on the FE performance determining factors.

Emitter Geometry

From the above discussions, it is very clear that the FE thereby field enhancement strongly depend on morphology and aspect ratio of the emitters. CNTs, the premier candidate in this

arena in general possess a high aspect ratio relying on which an excellent FE performance is resulted. To attain such quality emission performance high aspect ratio, proper arrangement as well as geometrical modification of ZnO nanostructure is highly desirable. In 2005, Cui et al.¹⁸⁸ have investigated the FE properties of ZnO nanowire arrays grown at 90 °C on polystyrene sphere, polyethylene foil, SiO₂ and Si wafers. Prior to this work there were only few reports on ZnO field emission and among them mostly proceed at high temperature vapor phase which made it a work of great importance. In the same year, Zhang et al.¹⁸⁹ have synthesized large-scale bi-layered ZnO nanorod arrays on Si substrate via chemical reaction in a dilute solution. Estimated β value for ZnO array with a diameter of 30 nm was 1680, larger than that of the ZnO array with a diameter of 100 nm. Such results suggested that reduction in diameter of the ZnO nanorod is critical for the improvement of the FE characteristics. 1D ZnO nanoneedles produced via electrochemical technique over Au coated Si showed moderate emission performance where the recorded turn-on field was $18.9 \text{ V } \mu\text{m}^{-1}$.¹⁹⁰ To attain high emission performance from geometrical modification of nanostructure became an art. Highly aligned ZnO nanotip arrays on ZnO films prepared by soft chemical route showed a turn-on field of about $10.8 \text{ V}/\mu\text{m}$ at current density of 0.1 mA cm^{-2} .¹⁹¹ Liu et al.⁴² have reported a comparison of FE performance of nanoneedles, hexagonal nanorods and nano-pencils which suggested highest β value for nanoneedle and nominal for hexagonal nanorod. Ye et al.¹⁹² have also compared the emission performance between standard ZnO nanorods and cone-like nanorod where ZnO nanorods with diameter $\sim 150 \text{ nm}$ showed poor emission. However modification of their tip radius down to $\sim 5 \text{ nm}$ enhanced the performance. Fascinating morphology like ZnO nanopillar and ZnO nanoflowers were synthesized by electrochemical deposition and employed for FE study. Detailed investigation on the FE of these nanoforms indicated that nano-pillars with high aspect ratio show good performance with a low turn-on field of $0.16 \text{ V } \mu\text{m}^{-1}$ and β value of 2.86×10^4 .¹⁹³ Along with similar nano-pillars, another type of 1D ZnO nanoform on ITO substrate namely nanospikes in the form of globular bunches were prepared by Pradhan et al.¹⁹⁴ In contrast to nano-pillars with flat tops, the nanospikes with tapered tips displayed improved emission performance, with a turn-on field of $3.2 \text{ V } \mu\text{m}^{-1}$ for $1.0 \mu\text{A cm}^{-2}$ and a threshold field of $6.6 \text{ V } \mu\text{m}^{-1}$ for 1.0 mA cm^{-2} . Assembly and integration of 1D nanostructure into complex geometry, especially in hierarchical form are also explored. To attain high emission performance, Cao et al.¹⁰⁹ also have studied the FE properties of different ZnO nanoforms and suggested emission supremacy for hierarchical ZnO nanowire array which was due to its high aspect ratio, small

radius curvature, and proper density. Jiang et al.¹⁹⁵ have registered a turn-on and threshold field of $\sim 3.7 \text{ V } \mu\text{m}^{-1}$ and $\sim 4.8 \text{ V } \mu\text{m}^{-1}$ respectively from urchin-like 3D ZnO nanostructures which were consisted of ZnO nanorods. Hierarchical ZnO nanostructures with nanorods engendered into pin-cushion cactus along with nano-pencils showed low turn on field of $\sim 1.38 \text{ V } \mu\text{m}^{-1}$.¹⁹⁶ Authors have explained such high emission on the basis of a sequential enhancement mechanism involving the consecutive stem and tip contribution. Besides 1D nanorod or nanowire or their assembly researchers has also used ZnO nanotube for FE. Wei et al.¹⁹⁷ have tested FE properties of hydrothermally grown ZnO nanotube arrays and registered a turn-on field of about $7.0 \text{ V}/\mu\text{m}$ at a current density of $0.1 \mu\text{A}/\text{cm}^2$. High FE performance not only ensured from the 1D nanostructure with sharp geometry, from 2D nanoforms also it was accounted. ZnO nano-walls prepared by Pradhan et al.⁹¹ on conducting ITO substrate exhibited excellent FE performance, with a considerably low turn-on field of $3.6 \text{ V } \mu\text{m}^{-1}$ (at $0.1 \mu\text{A cm}^{-2}$) and higher current density of 0.34 mA cm^{-2} at $6.6 \text{ V}\mu\text{m}^{-1}$. Recently our group⁴⁷ has examined the FE characteristics of an unusual 3D ZnO nanoform made of numerous nanosheets and compared the performance with 1D nanowire. Hierarchical sheet assemblies performed with much better stability and lower operating field (turn-on field $3.5 \text{ V } \mu\text{m}^{-1}$) as compared to the 1D counterpart. Surface modification of ZnO nanostructure is another way to achieve high emission performance. Recently we have designed a multistage field emitter based on graphene-linked ZnO nanowire array by means of spin-coating graphene dispersion on nanostructured platform followed by plasma modification.¹⁵⁵ The field values were downshifted compared to the individual components in cascade emitter. Facile electron transfer from nanowires to graphene due to band bending at ZnO–graphene interface together with multistage geometrical field enhancement remained behind this enriched field emission. Variation in FE characteristics due to the variation in emitter geometry is presented in Figure 7(a-d).^{40,109} Further, here we have presented some representative results on field electron emission of ZnO nanoform reported so far, with brief remarks on the emission field values in Table 2.

Inter Emitter Cross Talking

Field screening between the emitter or inter emitter cross talking is another pivotal factor which has strong influence on the overall β value determination. Particularly, screening of electric field by its neighbors largely influences the electron emission efficiency of individual nanostructures. Chen et al.²¹⁰ have described the dependence of β on the aspect ratio and

interspacing of the ZnO nanowires which can be written as $\beta_{ZnO} = b\left(\frac{L}{r} + h\right)^{0.9} [1 - \exp(-a\frac{s}{L})]$ where 'a' and 'b' are constant, 'L' and 'r' are the length and radius of the nanostructure, 'h' is a parameter used in fitting the experimental data. From this equation it is obvious that β value depends not only on the aspect ratio of nanowire but also largely on the interspacing ('s'). For a typical nanostructure, their number density, separation between themselves and alignment of the substrate determine the value of screening factor 'S'. In other words, field screening enumerates the interaction between nanostructures electronically, optically and mechanically. Further, a better insight into the extent of screening on β value can be feasible from the empirical expression for field screening factor ('S') put forwarded by Chen et al.²¹¹ which can be expressed as $S = \exp(-d/0.65L)$ where 'd' and 'L' are the distance of two nearest neighbored nanotubes and length of the nanotube respectively. Though the expression was used for CNT array however it can be used for other material also as it does not depend on material's intrinsic features. This expression indicated that close proximity of the field emitter may lead to very large value of screening factor 'S', thereby giving large negative influence on β value. Thus an appropriate density of the emitters and their alignment is crucial to achieve a high and uniform FE. Emission performance comparison between different types of multipod namely multipod-1 and multipod-2 with alike areal density by Ramgir et al.²¹² clearly indicated low onset voltage for the multipod which have low areal density (multipod-2). Due to low areal density field screening effect will be less in multipod - 2. This work clearly signified the importance of tuning the density of nanostructures, in order to achieve the advantage of low onset voltage offered by an individual nanostructure. Too high number density from an optimum value would lead to lowering of the emission current due to high screening. Then again, low density also pulled down the FE current density due lack of inadequate numbers of emitters. To overcome screening effect, number density controlled of the emitter becomes the hotspot of research. By varying the thickness of the seed layers Liu et al.²¹³ have controlled the density and diameter of nanowires in very subtle manner. Increment in seed layer thickness resulted in an increase in number density accompanied by a decrease in diameter. Further, faster decrement in diameter as compared to the same in height increases the aspect ratio of the nanowire when the density increases. Both changes in density and aspect ratio were found to affect the FE characteristics. Increase in aspect ratio not fully reflected in the improvement in FE as field screening effect came in to play owing to simultaneous increase in number density. Growth over pattern substrate and

thereby controlling the separation between emitters using lithography is another way to circumvent the screening issue. Lee et al.²¹⁴ have proposed a method to tune the FE properties of site-and area-density-controlled ZnO nanorod array using an aqueous process assisted by nanosphere lithography technique. They have observed lowest turn on field $\sim 2.98 \text{ V } \mu\text{m}^{-1}$ corresponding to current density of $10 \mu\text{m cm}^{-2}$ and highest β value of 1732 for the array with lowest areal density. Such performance by the particular sample was accredited to the adequate spacing between the nanorods and the high crystalline quality. Minimizing the field screening issue remarkable enhancement in field emission was also observed by observed by other group also.^{204,215} Though it is superficial from above discussion that only nanostructure with well alignment can render high emission performances due to low field screening however few reports suggested random orientation nanostructures could also produce similar result with optimal density.²¹⁶

Work function and conductivity

For the easiness of the electron emission from the emitter, the work function of the emitter must be low. In other word for certain applied electric field, material with low work function should exhibit high emission current density. ZnO possess a work function of 5.3 eV. In order to achieve high emission current density as well to attain low field values the work function should be reduced by any means. Doping of ZnO with trivalent materials like In, Ga or Al etc. is one possible way for the lowering of work function of ZnO. Doping not only increases the electron concentration it also creates an additional energy levels within the band gap of ZnO and thereby reduces the effective Φ value. Liu et al.²¹⁷ have synthesized highly ordered titanium (Ti) doped ZnO nanorod arrays which exhibited high β value and low field values. Reduction in work function due to widened energy bandgap combined with the upshift of the Fermi level in the n type Ti doped ZnO sample resulted such improved result compared to the undoped sample. Ye et al.²¹⁸ have fabricated In doped ZnO film and obtained relatively weak field emission result due to the increment of work function the doped film. Unintentional inclusion of acceptors like nitrogen and oxygen vacancies increases the work function of ZnO by reducing the electron density and lowering the Fermi level position of the doped film. Such result suggested that unintentional incorporation of acceptors should be avoided to decrease the work function of the emitters and hence to achieve better field emission. Decrement in work function also achieved via several other routes also. A few nanometer thick Au film on top of the ZnO nanowires was found to lower the electric field for electron

emission significantly while thicker ones have little effect on the field-emission properties.¹⁸⁸ Such enhancement is attributed to reduced work function and change in surface geometry after gold coating. Similar sort of work was also performed by Ye et al.¹⁹² Besides geometrical modification, they have decorated ZnO nanorod it by metal particles like Au and Ag. Local field enhancement near the tip of the nanorods and the lowering of work function of ZnO nanorods rendered high emission. Aside work function, electrical conductivity of the emitters play crucial role on FE. High electrical conductivity of the emitter eases the emission process and thereby renders high β value. Doping of ZnO with anion like Nitrogen (N₂) have ensured an increment in the field enhancement.²¹⁹ Nitrogen considered as superior acceptor dopant for ZnO as it enhances the p-type conductivity system. This enhancement in intrinsic conductivity resulted improved FE performances of doped samples. Electron field emission comparison of pure ZnO and Mg doped ZnO nanostructures by Razaie et al.²²⁰ suggested significant improvement with Mg doping where the enhancement were due to increase in electrical conductivity. Coating or organization of low work function material like CeO₂ with ZnO also resulted in high field enhancement.¹⁶⁴ CeO₂ nanoparticles attachment not only increase the number of emission sites it also enhanced the electrical conductivity. Enhancement in FE performance due to enhanced electrical conductance was also observed by Devarapalli et al.²²¹

Effect of underlying substrate

Electron emission ability from nanostructure, accounted for by field enhancement factor also depends on the underlying substrate. Similar sort of nanostructure, one realized over PET substrate coated with ITO and other on ITO coated glass substrate showed different emission performance where except the flexibility variance of substrates, all other parameters were remained quite identical.^{91,222} Though exact explanation remained still unclear yet this result indicated that substrate had a vital role to play in electron emission. Jo et al.²²³ have prepared ZnO nanowire on carbon cloth via vapor phase which showed exceptionally low field values. Our group has also synthesized ZnO nanowire with different aspect ratio on carbon fabrics through wet chemical process.⁶⁰ Optimized arrays of nanowires displayed ultralow turn-on as well as threshold field of 0.27 and 0.56 V μm^{-1} . According to Jo et al.²²³ the overall β value of a combined geometry field emitter is the product of the β values of the individuals can be express as $\beta_{\text{overall}} = \beta_{\text{ZnO}} \beta_{\text{cloth}}$. This additional booster field enhancement factor (β_{cloth}) to the nanowire field enhancement factor (β_{ZnO}) was the reason behind superior FE behavior

observed from the ZnO nanowires over carbon cloth. In another previous work we have examined the influence of the underlying substrate on FE characteristics of nanospike and the result is presented in Figure 8(a,b).⁴¹ Electron before the emission from the nanospike tip has travelled across the junction between substrate and base of nanospike where they faced an energy barrier due to formation of metal-semiconductor junction. Due to low energy barrier nanospikes on ITO and carbon cloth gave better FE performance as compared to others. Then again, junctions between nanospike and p-type silicon substrate get reverse biased and thus produced negative impact on electron emission.²²⁴ Further, it is also suggested that stable Ohmic contact at the substrate-nanoform interfaces has a significant impact on FE of ZnO nanostructures.^{225,226}

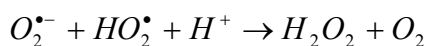
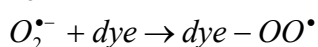
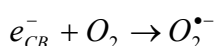
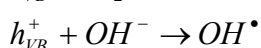
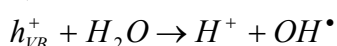
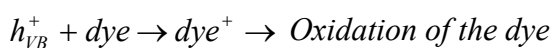
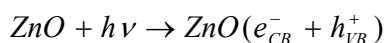
Not only the work function decrement or conductivity enhancement was resulted due to doping, researchers also suggested that with doping number of defects in nanoforms increases which have improved the emission process. FE performance investigation from Al-doped ZnO by Navale et al.²²⁷ revealed that with high Al doping percentage greater number of defects states formed which further acted as dominant emission sites at higher electric field. Aside to these, oxygen vacancy has significant impact on FE from ZnO nanostructures as verified experimentally by Zhao et al.²¹⁸ Surface defects like as oxygen vacancies behave as adsorption sites. Influence of oxygen vacancy in FE was elaborately discussed in our previous work.^{40,60} Annealing of ZnO nanostructure in oxygen atmosphere also resulted FE enhancement as oxygen annealing causes defect passivation namely oxygen vacancy defect whereas similar annealing treatment in air or ammonia have diverse effect on emission.²²⁸

Photocatalysis:

Ever increasing demand of clean water and simultaneous scarcity of its sources due to rapid urbanization and population growth, have become a concerning issue worldwide. With such ever growing demand, several strategies have been adopted for wastewater purification amid which heterogeneous photocatalysis employing metal oxide catalysts is widely accepted owing to its non-selectivity, high efficiency and cost effectiveness. Photocatalytic reaction takes place when the semiconductor catalyst is exposed to a light of energy higher or equal to the band gap energy of it. The basic criteria for an competent semiconductor photocatalyst is that the redox potential of charge carriers, i.e. e^-/h^+ must lies within the band gap of catalyst. The energy level at the bottom of conduction band actually determines the reducing ability of

photoelectrons whereas energy level at the top of valence band decides the oxidizing ability of photogenerated holes.²²⁹ Figure 9 depicts band edge positions of several semiconductors where the ordinate represents internal energy not free energy.²³⁰ Semiconductors like GaAs, PbS and CdS are not so stable for catalysis in aqueous media as they readily undergo photocorrosion and they are toxic also.²²⁹ On the other hand, Fe₂O₃, SnO₂ and WO₃ possess a conduction band edge at an energy level below the reversible hydrogen potential. Hence systems using these materials need an external electrical bias to complete the water splitting reaction and achieve hydrogen evolution at the cathode.²²⁹ Among all, TiO₂ is the most studied photocatalyst which shows high catalytic activity and is stable to incident photon or chemical corrosion. Next to TiO₂, ZnO is the widely used photocatalyst for degradation of pollutants. ZnO has added advantage over TiO₂ as it absorbs a larger fraction of the UV spectrum and the threshold wavelength ~ 387 nm.²³¹

ZnO has been broadly used as photocatalyst for producing charge carriers and thereby inducing oxidative and reductive processes, respectively. Usually, absorption of light by ZnO promotes an electron (e⁻) from the valence band to the conduction band, creating a positive hole (h⁺) in the valence band. These electrons in conduction band on the catalyst surface reduce the molecular oxygen to superoxide anion. This radical, in presence of organic scavengers, may form organic peroxides or hydrogen peroxide. Thus, in aerated aqueous suspension, oxygen is reduced to O₂^{•-} by electrons promoted in the conduction band. Electrons in the conduction band are also responsible for the production of hydroxyl radicals via oxidizing OH⁻ or H₂O by positive holes. These highly reactive species are the primary cause of organic matter mineralization due to the direct oxidation of pollutant dye molecule. A schematic of photocatalytic mechanism using ZnO is presented in Figure 10.²³² The photochemical assisted formation of some characteristic reactive groups (ROS) is presented in the following reaction sequence and the total procedure can be formulated as follows:²³²





Some of the frequently used dyes employed as the target substrates in the ZnO-assisted photocatalysis together with their absorption wavelength maxima are given are listed in Table 3. Further some photodegradation results shown by recently developed ZnO nanoforms and comment on these performances is presented in Table 4. The rate of decolorization is observed in terms of change in intensity at λ_{\max} of the dyes and the percentage of degradation

is calculated using the Beer Lambert relation: $\text{Degradation}(\%) = \frac{C_0 - C}{C_0} \times 100$ Where, C_0 is

the initial concentration of dye and C is the concentration of dye after photo irradiation. Typical UV-vis absorption spectra for different light exposure and digital image of the decoloration corresponding to various dyes are presented in Figure 11.^{140,231,240,241,247-251} The efficiency of ZnO nanostructure based photocatalysts depend on several parameters which will be discussed in the following section.

Surface area and morphological dependence on photocatalytic activity:

Morphology of ZnO nanoform plays a pivotal role in photocatalytic activity determination; this arises from the differences in surface area, population of polar planes and etc. With high surface area of the catalyst the probability of encountering electrons/holes with water/oxygen is greatly enhances which further leads to the high radical formation efficiency and high catalytic performance. In other words, if more number of atoms resides on nanoform surface, it enhances the adsorption capacity of the photocatalysts towards dye. Photocatalytic performance of ZnO can be improved by the realization of suitable geometric nanoforms with effective carrier transfer pathways. ZnO possess a rich assortment of nanoforms and those can be Control to desirable shape and consider for rational tailoring of the aspect ratio. Capabilities to tailor the nanostructure morphology and realization of the surface signatures of ZnO have broaden their potential usages. Zhai et al.²⁵² have studied the photocatalytic degradation study of methyl orange (MO) by various ZnO nanoforms and suggested different catalytic activity of them where the catalytic activity has been following the sequence: nanodisks> nanoparticles> hexagonal nanorings> microtyres. Such result indicated that the morphology and structure of the photocatalyst has an important influence on the degradation rate of MO. Significant impact of morphology on photocatalysis was further confirmed by several others also.^{119,253} One such comparison of photocatalytic activity of samples with different morphology under the same experimental conditions is illustrated in Figure 12a.²⁵³

Though it is superficial from the above discussion that only nanostructure with high surface area render high catalytic performances however few exceptions are documented in literature where high surface areas of the catalysts did not result in higher catalytic performance.^{253,254} Photocatalytic reaction mainly occurs at the interface between the catalyst surface and organic pollutant which clearly suggest that the growth direction of the crystal plane has strong impact on the photocatalytic activity of ZnO. Driven by such speculation researchers have explored the relationship between surface orientation of ZnO and their photocatalytic performance. Jang et al.²⁵⁵ have suggested that the polar Zn (0001) plane is the most active site for photocatalytic H₂O₂ generation. Photocatalytic comparison study of different nanoforms by them suggested highest activity by the ZnO plates among the synthesized nanoform which was due to the high population of polar Zn (0001) faces in it. Wang et al. also observed similar facet dependent catalytic performance differences.²⁵⁶

Effect of defect on photocatalysis:

Surface defect in ZnO has played an influential role in adsorption and surface reactivity. It is well accepted to achieve efficient photocatalytic activity, recombination time suppression of the photogenerated carriers in the catalyst is essential. In defect free ZnO, these photoexcited electrons and holes undergo quick recombination both on the surface and bulk of it whereas in case of ZnO with defect, the scenario is slightly complicated. ZnO nanostructure having defects in it facilitates the separation of photogenerated electron-hole pairs and can trap the photogenerated holes. Moreover these trapped holes are set to react with electron donors and the catalytic reaction is greatly upheld. Thus the intrinsic defect has a positive influence on the catalytic activity.²⁵⁷ Zhang et al.²⁵⁸ have investigated the relationship between structure and luminescence as well as photocatalytic property of low-dimensional ZnO nanocrystals. They found that the photocatalytic activity of the synthesized ZnO nanocrystals is mainly dependent on the type and concentration of oxygen defects. Photocatalytic activity measurement of ZnO nanocrystals with different oxygen defects (type and concentration) by Wang et al.²⁵⁹ suggested that the sample with higher amount of oxygen defects exhibits excellent activity toward the degradation of Rhodamine (RhB). There are various sorts of defects in ZnO among which doubly ionized oxygen vacancy acting as electron acceptors temporally trap photogenerated electrons and prevents the chance of energy-wasteful surface recombination of photogenerated electron-hole.¹²⁰ Though the defect dependent catalytic

reaction looks simple from above discussion however to achieve exact co-relation between these two further research is necessary.

Effect of catalyst concentration on degradation of dyes:

In photocatalytic processes, catalyst loading is a crucial parameter which has strong impact on degradation rate. The optimal catalyst dosage during the catalytic study relies on two factors: nature of the catalyst material and the photoreactor morphology.²⁶⁰ Increase in catalyst loading ensures the availability greater number of reaction site and thereby more hydroxyl radiation formation inside the solution. With more number of hydroxyl radical in the solution, photodegradation rate increases. On the other hand, catalyst loading over an optimum value has negative effect on degradation rate. Higher than the optimum value increases the turbidity of suspension and a reduction in light intensity throughout the solution occurs which further slowdown the degradation. Behnajady et al.²⁴⁰ has investigated the impact of catalyst dosage on the photocatalysis. With an increased ZnO loading from 150 to 750 mg L⁻¹ the percent of degradation increased from 49.1 to 92.98 at 60 min irradiation time. Catalyst loading for maximum degradation of 40 mg L⁻¹ of Acid Yellow 23 was 750 mg L⁻¹. After that the increase in catalyst loading paced down the degradation. Effect of catalyst loading on final decolorization was also examined by Ghule et al.^{260,261} Effect of catalyst loading on final decolorization was also tested by several other groups and few observed results are shown in Figure 12 b and c.^{240,260-262}

Effect of initial dye concentration:

Besides catalyst loading, dye dosage is also an important parameter in photocatalysis where the rate of decreases with the increase of dye concentration. With the increase of initial dye concentration the path length of the photon entering within the solution decreases and lesser number of photons can only reaches to the surface of catalyst. Such low photon density only excites few numbers of catalysts and decreases the formation of superoxide ion and hydroxyl radical, hence a decrement in degradation rate results. For a particular photocatalytic experiment with a fixed catalyst loading the catalyst surface area remain same, so with the increase in initial dye concentration the efficiency deccerses.²⁶³ Mohsin et al.²⁶⁴ have investigated the effect of initial dye concentration on photocatalysis study using commercial ZnO powder with particle size of 200 nm. Observed result suggested that in photocatalytic experiment with a fixed catalyst loading and other parameters the degradation rate decreases

with the increase in initial dye concentration. With a fixed surface area of catalyst high dye concentration results in only few active sites in the solution for the little adsorption dye molecules; leaving the remaining dye in solution. These remaining dye molecules can only destroy after the degradation of earlier attached molecules. Further at high concentration presence of huge number molecules face competition between themselves to attach at the active site which also result in slow degradation rate. Byrappa et al.²⁶³ have studied the effect of initial dye concentration in photodegradation of RhB and found that the efficiency of degradation decreased with the increase in initial dye concentration. Such impact of initial dye concentration on the photodegradation efficiency of RhB is presented in Figure 12d.²⁶³

Effect of pH:

pH value of the reaction medium is another key parameter in photodegradation study which can affect the adsorption of the hazardous dye on the catalyst surface. Additionally, the hydroxyl radical generation in photocatalytic reaction also depends on the pH of the solution.²⁶⁵ The effect of pH on photocatalysis is accounted due to the surface charge of catalyst and its relation with the ionic form of the dye.²⁶⁶ The point of zero charge of ZnO is about pH 8.9 beyond which the surface of ZnO catalyst become negative and below this point of zero charge (PZC) the surface are positively charged.²⁶⁷ Photodegradation is generally studied within the range from ~3 to 13 i.e. from acidic to basic for different types of dye like catatonic, anionic and neutral dyes. PH dependent photocatalytic study by Evgenidou et al.²⁶⁶ suggested enhancement in degradation rate with the sharp increase of pH from 2 to 7 and maximum degradation rate at pH 7 for ZnO. Further increase of pH resulted decrement in the degradation rate. Low initial reaction rate at acidic or alkali pH was due to dissolution and photodissolution of ZnO. Being an amphoteric oxide ZnO in acidic pH produces corresponding salt and at alkaline pH, it can react with a base to form complexes like $[\text{Zn}(\text{OH})_4]$. Benhebal et al.¹⁹ have examined the photocatalytic degradation of phenol and benzoic acid using ZnO powders and found that the degradation rate of both substrates was maximum at acidic pH and decreased with increasing pH. The effect of PH on the photo degradation efficiency of AR14 was examined in the range 4-12 in an aqueous ZnO suspension by Daneshvar et al.²³², where they have observed higher photodegradation efficiency in acidic solutions than the same in alkaline solutions. The as observed result is shown in Figure 12e.²³² pH dependent photocatalytic of ZnO also studied by other group also.^{240,268}

Effect of irradiation source:

Degradation percentage in photocatalysis can be improved with increase of exposed light intensity. Light irradiation with elevated intensity causes more electron-hole pair generation and thus makes it dominant over electron-hole recombination probability. Conversely, under the poor intensity of light illumination separation of the photogenerated carriers (electron/hole) competes with recombination of the same. As the consequence of this competition formation of hydroxyl radical decreases within the solution and poor degradation rate is result. Besides intensity of light, its wavelength is also important for photocatalytic study. Keeping the wavelength of light fixed (356 nm) Chakrabarti et al.²³³ have investigated the effect of light intensity in photocatalysis. For Eosin Y, extent of photo degradation decreased from 93 to 82% as the light intensity decreased from 0.1919 to 0.1048 $\mu\text{W}/\text{cm}^2$. Decrease in the number of photons generated with a reduced intensity of the lamp was the reason behind such decrement in photodegradation. The influence of light intensity on the degradation efficiency has also examined Behnajady et al.²⁴⁰ Figure 12f depicts the observed result which indicated the increase in percentage of decolorization and photodegradation with increasing the light intensity.²⁵² Not restricted to intensity variation, Saikia et al.¹¹² have studied the effect of different light sources on photodegradation of malachite green (MG) in presence of ZnO catalyst and the as obtained result is depicted in Figure 12g.¹¹² The observed result suggested highest degradation under UV light and nominal for the without catalyst case. Further, the results suggested degradation in solar light also however the efficiency weaker than the same in UV light.¹¹²

Enhancement of ZnO photocatalysis through modification:

Wide band gap of ZnO impede the effective utilization of entire solar spectrum as they only absorb the ultraviolet irradiation (4% of the solar light) consequence of which a poor photocatalytic behavior is accounted. To widen up the absorption range as well as to enhance the catalytic activity of ZnO, numerous protocols were adopted amid which coupling of one semiconductor with another semiconductor such as oxide or sulfide were the commonly accessed routes. Recently Pal et al. has been reported the fabrication of an oxide based nanostructure hybrid has been realized by integrating low bandgap CuO nanosheet with high bandgap 1D ZnO nanowires on a flexible carbon cloth as well as on a flat substrate.¹⁵⁶ These bandgap modulated hybrid nanostructures are generated for the efficient absorption of visible

light, targeting their possible use in waste water management. Environmental remediation through catalytic activity under the visible light irradiation of the synthesized samples was inspected using both anionic and cationic dyes (methyl orange and Rhodamine B, respectively) as model contaminants, where the optimized heterostructure exhibits significantly better performance than the mono component oxides. Such enhanced performance was explained on the basis of favourable staggered gap multiple p–n junctions at ZnO/CuO interface, which in turn retarded the photogenerated electron–hole pair recombination within the heterostructure.¹⁵⁶ Photocatalytic reduction process by ZnO/CuO heterostructure under visible light illumination is schematically shown in Figure 13. By realizing NiO/ZnO heterojunction Luo et al.¹⁷¹ have also achieved excellent catalytic performance, where the formation heterojunction improved the separation rate of photogenerated electrons and holes and enhanced photocatalytic efficiency. Scientists have also attached several metals like Pt, Ag etc. with ZnO or doped it with suitable metals like La, Mn, Co etc.²⁶⁹ to achieve higher photodegradation performances. Photocatalytic tests of Pt-ZnO microspheres for the degradation of acid orange II revealed extremely high photocatalytic activity and stability where the enhancement was originated from their unique nanostructures and the low recombination rate of the e^-/h^+ pairs by the Pt nanoparticles embedded in ZnO nanocrystals.²⁷⁰ Besides these metal combination, graphene-ZnO amalgamation also showed their propitious as an efficient photocatalyst.²⁷¹

Conclusions and outlook:

We have comprehensively reviewed the recent developments on low temperature solution processed dimension controlled ZnO nanoforms and their usage perspective as electron field emitter and photocatalyst. With judicious choice of experimental techniques and proper starting material and growth conditions, tailored nanoforms with different dimensionality were achieved by the researchers. Not just regular survey on the field emission and photocatalysis performance of ZnO nanoforms have done in this article, elaborate discussion on the other related issues which has profound impact over these performances were also made. Above discussions suggest strong impact of emitter geometry, emitter organization, work function of the emitter material on electron field emission of the solution processed nanoforms. Then again, photocatalytic performance is largely governed by the nanoform morphology thereby its overall surface area and defect constitution. Such facile realization of nanoforms by environmentally benign low temperature synthesis approaches enabled them to

assimilate with vast range of materials and made them fitted as unique building blocks to integrate in modern electronic and optoelectronic devices.

Although encouraging progress has been already accomplished on the research of ZnO nanostructures, still there are numerous of unsolved problems and scope for innovation. Firstly, low temperature solution ZnO nanostructures usually exhibit low crystal quality due to unintentional defect incorporation in the forms of point defects and voids etc. Such defects result low carrier mobility, low fracture toughness, short carrier life time and largely undermine the electrical, optical and mechanical properties. For crystal quality improvement of the low temperature, chemically synthesized nanostructures; serious attention has to be paid immediately. Choice of well controlled reaction parameter, suitable precursor, control over apparently minor issues and introduction of some capping agent during growth could be the possible ways to circumvent the above issues. Secondly, another challenge is the attainment of good p-type electrical conductivity of ZnO comparable to their n-type counterpart. Though p type conductivity for ZnO is feasible, it still remain a hurdle for researchers to dope ZnO with proper group I or group IV elements. Reaction involves the doping of foreign atom in ZnO is entropically favorable however reverse enthalpically.¹³ Proper choice element with similar ionic radius, similar electronegativity and controlled reaction parameters for minimum enthalpy change is highly desirable in this regard. Further, documentation on such type of doping are very few in number and most of them were achieved at high temperature; thus there is an enormous opening to work on low temperature solution phase doping. From above discussion it is obvious that along with nanostructure morphology, their arrangement over substrate has major role in performance determination. Experimental protocols reported to produce uniform ZnO nanostructure array with require density are mostly achieved by using sophisticated lithographic techniques which limits its practical usage. Production of pattern with accuracy and thereafter realization of nanoform array over it totally by budgetary low temperature approach is highly desirable. Biological application of these low temperature solution processed nanoforms is another less cultivated area thus calls for a thoughtful research in this regard. Finally, despite rigorous laboratory research work, realization of devices on industrial scale for the practical usage of human being is still lacking which demands for serious attention.

Author Contributions:

*S.M. and S.P. contributed equally to this work.

Acknowledgements:

The authors also wish to thank the University Grants Commission (UGC) for financial support under ‘University with Potential for Excellence (UPEII)’ scheme. One of us ‘S.P.’ wishes to thank the Council of Scientific and Industrial Research (CSIR), Government of India, for awarding her a Senior Research Fellowship (SRF) during the execution of the work. The authors also wish to thank Dr. Kaustav Bhattacharjee for his kind support.

Reference:

1. U. Ozgur, Y. I. Alivov, C. Liu, A. Teke, M. A. Reshchikov, S. Dogan, V. Avrutin, S. J. Cho and H. Morkoc, *J. Appl. Phys.*, 2005, 98, 041301.
2. D. C. Look, *Mat. Sci. Eng. B-Adv.*, 2001, 80, 383.
3. Y. W. Heo, D. P. Norton, L. C. Tien, Y. Kwon, B. S. Kang, F. Ren, S. J. Pearton and J. R. LaRoche, *Mat. Sci. Eng. R*, 2004, 47, 147.
4. Z. L. Wang, *J. Nanosci. Nanotechno*, 2008, 8, 27.
5. Z. L. Wang, *Chinese Sci. Bull.*, 2009, 54, 4021.
6. M. H. Huang, S. Mao, H. Feick, H. Q. Yan, Y. Y. Wu, H. Kind, E. Weber, R. Russo and P. D. Yang, *Science*, 2001, 292, 1897.
7. W. I. Park and G. C. Yi, *Adv. Mater.*, 2004, 16, 87.
8. D. S. Mao, X. Wang, W. Li, X. H. Liu, Q. Li and J. F. Xu, *J. Vac. Sci. Technol. B*, 2002, 20, 278.
9. T. Y. Wei, P. H. Yeh, S. Y. Lu and Z. L. Wang, *J. Am. Chem. Soc.*, 2009, 131, 17690.
10. M. Law, L. E. Greene, J. C. Johnson, R. Saykally and P. D. Yang, *Nat. Mater.*, 2005, 4, 455.
11. Z. L. Wang and J. H. Song, *Science*, 2006, 312, 242.
12. Z. L. Wang, *Mater. Today*, 2007, 10, 20.
13. S. Xu and Z. L. Wang, *Nano Res.*, 2011, 4, 1013.
14. B. Weintraub, Z. Zhou, Y. Li and Y. Deng, *Nanoscale*, 2010, 2, 1573.
15. A. S. Lanje, S. J. Sharma, R. S. Ningthoujam, J. -S. Ahn and R. B. Pode, *Adv. Powder Technol.*, 2013, 24, 331.
16. Y. Wang, C. Zhang, S. Bi and Guangsheng Luo, *Powder Technol.*, 2010, 202, 130.
17. A. K. -Radzimska and T. Jesionowski, *Materials*, 2014, 7, 2833.

18. P. Li, Y. Wei, H. Liu; X. K. Wang, *J. Solid State Chem.* 2005, 178, 855.
19. H. Benhebal, M. Chaib, T. Salomon, J. Geens, A. Leonard, S. D. Lambert, M. Crine and B. Heinrichs, *Alex. Eng. J.*, 2013, 52, 517.
20. M. Ristić, S. Musić, M. Ivanda, S. Popović, *J. Alloy. Compd.*, 2005, 39, L1.
21. A. B. Djurišić, X. Y. Chen and Y. H. Lung, *Recent Pat. Nanotechnol.*, 2012, 6, 124.
22. T. Tsuzuki, H. Dawkins, J. Dunlop, G. Trotter, M. Nearn and P. G. McCormick, *Cosmet. Aeorosol Toilet. Aust.*, 2002, 15, 10.
23. D. Chen, X. Ciao and G. Cheng, *Solid State Commun.*, 2000, 113, 363.
24. A. A. Ismail, A. E. -Midany, E.A. Abdel-Aal and H. E. -Shall, *Mater. Lett.*, 2005, 59, 1924.
25. S. Musić, D. Dragčević, S. Popović and M. Ivanda, *Mater. Lett.*, 2005, 59, 2388.
26. T. Choduba, W. Łojkowski, E. Reszke and T. Strachowski, *US3450617 A*, 2009.
27. J. J. Schneider, R. C. Hoffmann, J. Engstler, A. Klyszcz, E. Erdem, P. Jakes, R. A. Eichel, L. P. -Bauermann and J. Bill, *Chem. Mater.*, 2010, 22, 2203.
28. J. Zhang, J. Wang, S. Zhou, K. Duan, B. Feng, J. Weng, H. Tang and P. Wu, *J. Mater. Chem.*, 2010, 20, 9798.
29. S. J. Chen, L. H. Li, X. T. Chen, Z. Xue, J. M. Hong and X. Z. You, *J. Cryst. Growth*, 2003, 252, 184.
30. O. Dulub, L. A. Boatner and U. Diebold, *Surf. Sci.*, 2002, 519, 201.
31. S. Yamabi and H. Imai, *J. Mater. Chem.*, 2002, 12, 3773.
32. B. G. Wang, E. W. Shi and W. Z. Zhong, *Cryst. Res. Technol.*, 1997, 32, 659.
33. L. N. Demianets, D. V. Kostomarov, *Ann. Chim. Sci Mat*, 2001, 26, 193.
34. L. N. Dem'yanets, D. V. Kostomarov, and I. P. Kuz'mina, *Inorg. Mater.*, 2002, 38, 124.
35. Q. Tang, W. J Zhou, J. M. Shen, W. Zhang, L. F. Kong and Y. T. Qian, *Chem. Commun.*, 2004, 712.
36. B. Cheng and E. T. Samulski, *Chem. Commun.*, 2004, 986.
37. M. Yin, Y. Gu, I. L. Kuskovsky, T. Andelman, Y. Zhu, G. F. Neumark and S.O' Brien, *J. Am. Chem. Soc.*, 2004, 126, 6206.
38. X. Wu, H. Bai, C. Li, G. Lu and G. Shi, *Chem. Commun.*, 2006, 1655.
39. Q. Li, K. Cheng, W. Weng, C. Song, P. Du, G. Shen and G. Han, *Nanoscale Res. Lett.*, 2011, 6, 477.
40. S. Maiti, U. N. Maiti, A. Chowdhury and K. K. Chattopadhyay, *CrystEngComm*, 2014, 16, 1659.

41. U. N. Maiti, S. Maiti, S. Goswami, D. Sarkar and K. K. Chattopadhyay, *CrystEngComm*, 2011,13, 1976.
42. J. Liu, X. Huang, Y. Li, X. Ji, Z. Li, X. He, and F. Sun, *J. Phys. Chem. C*, 2007, 111, 4990.
43. Y. Tak and K. Yong, *J. Phys. Chem. B*, 2005, 109, 19263.
44. Y. Gao, M. Nagai, T.-C. Chang and J. -J. Shyue, *Cryst. Growth Des.*, 2007, 7, 2467.
45. S. Baruah and J. Dutta, *Sci. Technol. Adv. Mater.*, 2009, 10, 013001.
46. K. Govender, D. S. Boyle, P. B. Kenway and P. O'Brien, *J. Mater. Chem.*, 2004, 14, 2575.
47. S. Maiti, U. N. Maiti and K. K. Chattopadhyay, *CrystEngComm*, 2012, 14, 8.
48. M. N. R. Ashfold, R. P. Doherty, N. G. N.-Angwafor, D. J. Riley and Y. Sun, *Thin Solid Films*, 2007, 515, 8679.
49. L. Vayssieres, *Adv. Mater.*, 2003, 15, 464.
50. S. H. Jung, E. Oh, K. H. Lee, W. Park and S. H. Jeong, *Adv. Mater.*, 2007, 19, 749.
51. H. E. Unalan, P. Hiralal, N. Rupesinghe, S. Dalal, W. I. Milne and G. A. J. Amaratunga, *Nanotechnology*, 2008, 19, 255608.
52. L. Shi, K. Y. Bao, J. Cao and Y. T. Qian, *CrystEngComm*, 2009, 11, 2009.
53. C. Cheng, B. Yan, S. M. Wong, X. Li, W. Zhou, T. Yu, Z. Shen, H. Yu and Hong Jin Fan, *ACS Appl. Mater. Interfaces*, 2010, 2, 1824.
54. Y. P. Fang, Q. Pang, X. G. Wen, J. N. Wang and S. H. Yang, *Small*, 2006, 2, 612.
55. S. H. Ko, D. Lee, H. W. Kang, K. H. Nam, J. Y. Yeo, S. J. Hong, C. P. Grigoropoulos and H. J. Sung, *Nano Lett.*, 2011, 11, 666.
56. Y. Yang, Y. Chu, Y. Zhang, F. Yang and J. Liu, *J. Solid State Chem.*, 2006, 179, 470.
57. S. Xu, Y. Wei, M. Kirkham, J. Liu, W. Mai, D. Davidovic, R. L. Snyder and Z. L. Wang, *J. Am. Chem. Soc.*, 2008, 130, 14958.
58. T.-Y. Liu, H.-C. Liao, C.-C. Lin, S.-H. Hu, and S.-Y. Chen, *Langmuir*, 2006, 22, 5804.
59. Y. Tang, X. Hu, M. Chen, L. Luo, B. Li and L. Zhang, *Electrochim. Acta*, 2009, 54, 2742.
60. U. N. Maiti, S. Maiti, R. Thapa and K. K. Chattopadhyay, *Nanotechnology*, 2010, 21, 505701.
61. C. Y. Jiang, X. W. Sun, K. W. Tan, G. Q. Lo, A. K. K. Kyaw and D. L. Kwong, *Appl. Phys. Lett.*, 2008, 92, 143101.
62. S. Xu, Y. G. Wei, J. Liu, R. Yang and Z. L. Wang, *Nano Lett.*, 2008, 8, 4027.
63. Y. Qin, X. D. Wang and Z. L. Wang, *Nature*, 2008, 451, 809.
64. C. S. Hsiao, C. H. Peng, S. Y. Chen, S. C. Liou, *J. Vac. Sci. Technol. B*, 2006, 24, 288.
65. L. -W. Ji, S. -M. Peng, J. -S. Wu, W. -S. Shih, C. -Z. Wu and I. -T. Tang, *J. Phys. Chem. Solids*, 2009, 70, 1359.

66. L. E. Greene, M. Law, D. H. Tan, M. Montano, J. Goldberger, G. Somorjai and P. D. Yang, *Nano Lett.*, 2005, 5, 1231.
67. H. Yang, Y. Song, Li Li, J. Ma, D. Chen, S. Mai and H. Zhao, *Cryst. Growth Des.*, 2008, 8, 1039.
68. B. S. Kang, S. J. Pearton and F. Ren, *Appl. Phys. Lett.*, 2007, 90, 083104.
69. B. Weintraub, Y. Deng and Z. L. Wang, *J. Phys. Chem. C*, 2007, 111, 10162.
70. C. Li, G. S. Hong, P. W. Wang, D. P. Yu, L. M. Qi, *Chem. Mater.*, 2009, 21, 891.
71. H. H. Solak, C. David, J. Gobrecht, V. Golovkina, F. Cerrina, S. O. Kim and P. F. Nealey, *Microelectron. Eng.*, 2003, 67, 56.
72. F. Claeysens, A. Klini, A. Mourka, C. Fotakis, *Thin Solid Films*, 2007, 515, 8529.
73. Q. Ahsanulhaq, J.-H. Kim and Y.-B. Hahn, *Nanotechnology*, 2007, 18, 485307.
74. Z. Zheng, Z. S. Lim, Y. Peng, L. You, L. Chen and J. Wang, *Sci. Rep.*, 2013, 3, 2434.
75. S. Peulon and D. Lincot, *Adv. Mater.*, 1996, 8, 166.
76. M. Izaki and T. Omi, *Appl. Phys. Lett.*, 1996, 68, 2439.
77. R. Konenkamp, K. Boedecker, M. C. Lux-Steiner, M. Poschenrieder, F. Zenia, C. Levy-Clement and S. Wagner, *Appl. Phys. Lett.*, 2000, 77, 2575.
78. J. Elias, R. T.-Zaera and C. L.-Clement, *J. Electroanal. Chem.*, 2008, 621, 171.
79. L. F. Xu, Y. Guo, Q. Liao, J. P. Zhang and D. S. Xu, *J. Phys. Chem. B*, 2005, 109, 13519.
80. R. T.-Zaera, J. Elias, G. Wang and C. L.-Clement, *J. Phys. Chem. C*, 2007, 111, 16706.
81. J. Elias, R. T. -Zaera and C. Levy-Clement, *J. Phys. Chem. C*, 2008, 112, 5736.
82. Y. Li, G. W. Meng, L. D. Zhang and F. Phillipp, *Appl. Phys. Lett.*, 2011, 76, 2000.
83. Y. Xi, C. G. Hu, X. Y. Han, Y. F. Xiong, P. X. Gao, G. B. Liu, *Solid State Commun.*, 2007, 141, 506.
84. J. H. Yang, G. M. Liu, J. Lu, Y. F. Qiu and S. H. Yang, *Appl. Phys. Lett.*, 2007, 90, 103109.
85. Z. Wang, X. F. Qian, J. Yin and Z. K. Zhu, *Langmuir*, 2004, 20, 3441.
86. B. I. Seo, U. A. Shaislamov, M. H. Ha, S.-W. Kim, H.-K. Kim, B. Yang, *Phys. E*, 2007, 37, 241.
87. C. Wang, B. Mao, E. Wang, Z. Kang, C. Tian, *Solid State Commun.*, 2007, 141, 620.
88. A. L. Yang and Z. L. Cui, *Mater. Lett.*, 2006, 60, 2403.
89. Z. R. Tian, J. A. Voigt, J. Liu, B. McKenzie, M. J. Mcdermott, M. A. Rodriguez, H. Konishi and H. Xu, *Nat. Mater.*, 2003, 2, 821.

90. B. Illy, B. A. Shollock, J. L. MacManus-Driscoll and M. P. Ryan, *Nanotechnology*, 2005, 16, 320.
91. D. Pradhan, M. Kumar, Y. Ando and K.T. Leung, *Nanotechnology*, 2008, 19, 035603.
92. D. Pradhan and K. T. Leung, *J. Phys. Chem. C*, 2008, 112, 1357.
93. J. P Cheng, Z. M. Liao, D. Shi, F. Liu and X. B. Zhang, *J. Alloys Compd.*, 2009, 480, 741.
94. T. R. Zhang, W. J. Dong, M. K.-Brewer, S. Konar, R. N. Njabon, Z. R. Tian, *J. Am. Chem. Soc.*, 2006, 128, 10960.
95. Y. Zhang, J. Xu, Q. Xiang, H. Li, Q. Pan and P. Xu, *J. Phys. Chem. C*, 2009, 113, 3430.
96. H.-M. Cheng, W.-H. Chiu, C.-H. Lee, S.-Y. Tsai and W.-F. Hsieh, *J. Phys. Chem. C*, 2008, 112, 16359.
97. V. Pachauri, K. Kern and K. Balasubramanian, *Chem. Phys. Lett.*, 2010, 498, 317.
98. H. Zhang, J. Wu, C. Zhai, N. Du, X. Ma and D. Yang, *Nanotechnology*, 2007, 18, 455604.
99. M. Chen, Y. Wang, L. Song, P. Gunawan, Z. Zhong, X. She and F. Su, *RSC Adv.*, 2012, 2, 4164.
100. X. Wang, W. Liu, J. Liu, F. Wang, J. Kong, S. Qiu, C. He and L. Luan, *ACS Appl. Mater. Interfaces*, 2012, 4, 817.
101. M. Wang, Y. Zhang, Y. Zhou, F. Yang, E. J. Kim and S. H. Hahn and S. G. Seong, *CrystEngComm*, 2013, 15, 754.
102. Y. Shi, C. Zhu, L. Wang, C. Zhao, W. Li, K. K Fung, T. Ma, A. Hagfeldt and N. Wang, *Chem. Mater.*, 2013, 25, 1000.
103. F. Xu, M. Dai, Y. Lu and L. Sun, *J. Phys. Chem. C*, 2010, 114, 2776.
104. X. G. Han, Y. Q. Jiang, S. F. Xie and Q. Kuang, *J. Phys. Chem. C*, 2010, 114, 10114.
105. H. I. Abdulgafour, F. K. Yam, Z. Hassan, K. AL-Heuseen and M. J. Jawad, *J. Alloys Compd.*, 2011, 509, 5627.
106. R. B. Kale, S. -Y. Lu, *J. Alloys Compd.*, 2013, 579, 444.
107. F. Zhao, J.-G. Zheng, X. Yang, X. Li, J. Wang, F. Zhao, K. S. Wong, C. Liang and M. Wu, *Nanoscale*, 2010, 2, 1674.
108. S. Zhu, L. Shan, X. Chen, L. He, J. Chen, M. Jiang, X. Xie and Z. Zhou, *RSC Adv.*, 2013, 3, 2910.
109. B. Cao, X. Teng, S. H. Heo, Y. Li and S.O. Cho, G. Li and W. Cai, *J. Phys. Chem. C*, 2007, 111, 2470.

110. M. R. Alenezi, S. J. Henley, N. G. Emerson and S. R. P. Silva, *Nanoscale*, 2014, 6, 235.
111. L. Xu, Q. Chen and D. Xu, *J. Phys. Chem. C*, 2007, 111, 11560.
112. L. Saikia, D. Bhuyana, M. Saikia, B. Malakara, D. K. Dutta and P. Sengupta, *Appl. Catal., A*, 2015, 490, 42.
113. Z. Xingfu, H. Zhaolin, F. Yiqun, C. Su, D. Weiping and X. Nanping, *J. Phys. Chem. C*, 2008, 112, 11722.
114. Y. Sun, L. Wang, X. Yu and K. Chen, *CrystEngComm*, 2012, 14, 3199.
115. B. Liu and H. C. Zeng, *Chem. Mater.*, 2007, 19, 5824.
116. S.-S. Wang and A.-W. Xu, *CrystEngComm*, 2013, 15, 376.
117. M. Mo, J. C. Yu, L. Zhang and S.-K.A. Li, *Adv. Mater.*, 2005, 17, 756.
118. X. Cao, N. Wang, X. Huang, Q. Feng, L. Wang, K. Zhou, X. Gao and J.-H. Lee, *CrystEngComm*, 2013, 15, 1715.
119. D. Kim and Y. -D. Huh, *Mater. Lett.*, 2011, 65, 2100.
120. A. K. -Radzimska, T. Jesionowski and A. Krysztafkiewicz, *Physicochem. Probl. Miner. Process.*, 2010, 44, 93.
121. T. Toyama, H. Takeuchi, D. Yamaguchi, H. Kawasaki, K. Itatani, and H. Okamoto, *J. Appl. Phys.*, 2010, 108, 084302-1.
122. L. N. Dem'Yanets, L.E. Li and T.G. Uvarova, *J. Mater. Sci.*, 2006, 41, 1439.
123. X. L. Hu, Y. -J. Zhu and S. -W. Wang, *Mater. Chem. Phys.*, 2004, 88, 421.
124. S.-H. Yi, S.-K. Choi, J.-M. Jang, J.-A. Kim and W.-G. Jung, *J. Colloid Interface Sci.*, 2007, 313, 705.
125. M. E. Fragalà, Y. Aleeva and G. Malandrino, *Superlattices Microstruct.*, 2010, 48, 408.
126. J. Yang, J. Lang, L. Yang, Y. Zhang, D. Wang, H. Fan, H. Liu, Y. Wang and M. Gao, *J. Alloys Compd.*, 2008, 450, 521.
127. R. Zhang and L. L. Kerr, *J. Solid State Chem.*, 2007, 180, 988.
128. C. X. Xu, X. W. Sun, S. N. Fang, X. H. Yang, M. B. Yu, G. P. Zhu and Y. P. Cui. *Appl. Phys. Lett.*, 2006, 88, 161921-3.
129. F. Xu, Y. Lu, L. Sun and L. Zhi. *Chem. Commun.*, 2010, 46, 3191.
130. Z. Wang, B. Huang, X. Qin, X. Zhang, P. Wang, J. Wei, J. Zhan, X. Jing, H. Liu, Z. Xu, H. Cheng, X. Wang and Z. Zheng, *Mater. Lett.*, 2009, 63, 130.
131. C. Y. Lee, T. Y. Tseng, S. Y. Li and P. Lin, *Nanotechnology*, 2006, 17, 83.
132. S. Lee, E. Lee and C. E. Lee, S. J. Noh and H. S. Kim, *J. Korean Phys. Soc.*, 2011, 58, 894.

133. B. Liu and H. C. Zeng, *J. Am. Chem. Soc.*, 2003, 125, 4430.
134. W. Jia, S. Dang, H. Liu, Z. Zhang, C. Yu, X. Liu and B. Xu, *Mater. Lett.*, 2012, 82, 99.
135. Z. M. Khoshhesab, M. Sarfaraz and Z. Houshyar, *Synth. React. Inorg. Met. Org. Nano Met. Chem.*, 2012, 42, 1363.
136. P. Li, Y. Wei, H. Liu, X. K. Wang, *J. Solid State Chem.*, 2005, 178, 855.
137. B. Sun and H. Sirringhaus. *Nano Lett.*, 2005, 12, 2408.
138. M.H. Mamat, Z. Khusaimi, M.Z. Musa, M.Z. Sahdan, M. Rusop, *Mater. Lett.*, 2010, 64, 1211.
139. T. Ghoshal, S. Kar and S. Chaudhuri, *J. Cryst. Growth*, 2006, 293, 438.
140. U. N. Maiti, S. Maiti and K. K. Chattopadhyay, *CrystEngComm*, 2012, 14, 640.
141. S. Cho, J. -W. Jang, J. S. Lee and K. -H. Lee, *Nanoscale*, 2010, 2, 2199.
142. Q. Li, J. Bian, J. Sun, J. Wang, Y. Luo, K. Sun and D. Yu, *Appl. Surf. Sci.*, 2010, 256, 1698.
143. Z. Cao, Z. Zhang, F. Wang and G. Wang, *Colloids Surf. A Physicochem. Eng. Asp.*, 2009, 340, 161.
144. K.V. Gurav, V. J. Fulari, U. M. Patil, C. D. Lokhande and O.-S. Joo, *Appl. Surf. Sci.*, 2010, 256, 2680.
145. C. Wu, X. Qiao, L. Luo and H. Li, *Mater. Res. Bull.*, 2008, 43, 1883.
146. Z. Z. Xu, Y. Ben, Z. L. Chen and F. Qi, *Mater. Res. Bull.*, 2013, 48, 1725.
147. H. Gao, F. Yan, J. Li, Y. Zeng and J. Wang, *J. Phys. D: Appl. Phys.*, 2007, 40, 3654.
148. A. Pan, R. Yu, S. Xie, Z. Zhang, C. Jin and B. Zou, *J. Cryst. Growth*, 2005; 282, 165.
149. Y. Wang, X. Li, G. Lu, G. Chen and Y. Chen, *Mat. Lett.*, 2008, 62, 2359.
150. K. M. Kumra, B. K. Mandal, E. A. Naidu, M. Sinha, K. S. Kumar and P. S. Reddy, *Spectrochim. Acta Part A Mol. Biomol. Spectrosc.*, 2013, 104, 171.
151. B. I. Kharisov. *Nanotechnology*, 2008, 2, 190.
152. J. Ge, B. Tang, L. Zhuo and Z. Shi, *Nanotechnology*, 2006, 17, 1316.
153. Y. Jiang, M. Wu, X. Wu, Y. Sun and H. Yin, *Mater. Lett.*, 2009, 63, 275.
154. C. C. Li, X. M. Yin, Q. H. Li and T. H. Wang, *CrystEngComm*, 2011, 13, 1557.
155. U. N. Maiti, S. Maiti, T. P. Majumder and K. K. Chattopadhyay, *Nanotechnology*, 2011, 22, 505703.
156. S. Pal, S. Maiti, U. N. Maiti and K. K. Chattopadhyay, *CrystEngComm*, 2015, 17, 1464.

157. F. Xu, Y. Yuan, H. Han, D. Wu, Z. Gao and K. Jiang, *CrystEngComm*, 2012, 14, 3615.
158. N. Wang, C. Sun, Y. Zhao, S. Zhou, P. Chen and L. Jiang, *J. Mater. Chem.*, 2008, 18, 3909.
159. H. He, W. Cai, Y. Lin and B. Chen, *Langmuir*, 2010, 26, 8925.
160. M. Deo, D. Shinde, A. Yengantiwar, J. Jog, B. Hannoyer, X. Sauvage, M. More and S. Ogale, *J. Mater. Chem.*, 2012, 22, 17055.
161. S. Yuyang, J. Long, Z. Tian, W. Jin, L. Ling, J. Yong, J. Zhifeng and S. Xiaosong, *New J. Chem.*, 2015, 39, 2943.
162. X. Sun, Q. Li, Y. Lü and Y. Mao, *Chem. Commun*, 2013, 49, 4456.
163. C. Cheng, B. Liu, H. Yang, W. Zhou, L. Sun, R. Chen, S. F. Yu, J. Zhang, H. Gong, H. Sun and H. J. Fan, *ACS Nano*, 3, 3069.
164. S. S. Warule, N. S. Chaudhari, B. B. Kale, K. R. Patil, P. M. Koinkar, M. A. More and R. -i. Murakami, *J. Mater. Chem.*, 2012, 22, 8887.
165. X. Wang, H. Zhu, Y. Xu, H. Wang, Y. Tao, S. Hark, X. Xiao and Q. Li, *ACS Nano*, 2010, 4, 3302.
166. S. Guo , D. Bao , S. Upadhyayula , W. Wang , A. B. Guvenc , J. R. Kyle , H. Hosseinibay , K. N. Bozhilov , V. I. Vullev , C. S. Ozkan and Mihrimah Ozkan, *Adv. Funct. Mater.*, 2013, 23, 5199.
167. J. Kim, W. Kim and K. Yong, *J. Phys. Chem. C*, 2012, 116, 15682.
168. W. W. Wang, Y. J. Zhu and L. X. Yang, *Adv. Funct. Mater.*, 2007, 17, 59.
169. G. K. Lau, T. S. Zhang, G. K. L. Goh, *J. Nanosci. Nanotechnol.*, 2010, 10, 4733.
170. S. Panigrahi and D. Basak, *Nanoscale*, 2011, 3, 2336.
171. C. Luo, D. Li, W. Wu, Y. Zhang and C. Pan, *RSC Adv.*, 2014, 4, 3090.
172. M. Lee and K. Yong, *Nanotechnology*, 2012, 23, 194014.
173. Y. F. Zhu, G. H. Zhou, H. Y. Ding, A. H. Liu, Y. B. Lin and Y. W. Dong, *Superlattices Microstruct.*, 2011, 50, 549.
174. Y. Wang, Q. Guo, S. Lin B. Chen and D. Zheng, *J. Phys.: Conf. Ser.*, 2009, 152, 012018.
175. Y. Bu, Z. Chen, W. Li and B. Hou, *ACS Appl. Mater. Interfaces*, 2013, 5, 12361.
176. W. D. Zhang, *Nanotechnology*, 2006, 17, 1036.
177. F. R. Fan, Y. Ding, D. Y. Liu and Z. Q. Tian, *J. Am. Chem. Soc.*, 2009, 131, 12036.

178. Y. Zhang, J. Xu, P. Xu, Y. Zhu, X. Chen and W. Yu, *Nanotechnology*, 2010, 21, 285501.
179. S. -M. Park, T. Ikegami, K. Ebihara, P. -K. Shinc, *Appl. Surf. Sci.*, 2006, 253, 1522.
180. J. B. Cui, Y. C. Soo, T. P. Chen and U. J. Gibson, *J. Phys. Chem. C*, 2008, 112, 4475.
181. T.-H. Fang and S.-H. Kang, *J. Nanosci. Nanotechnol.*, 2010, 10, 405.
182. S. B. Majumder, M. Jain, P. S. Dobal and R. S. Katiyar, *Mater. Sci. Eng. B*, 2003, 103, 16.
183. S. Cimitan, S. Albonetti, L. Forni, F. Peri and D. Lazzari, *J. Colloid Interface Sci.*, 2009, 329, 73.
184. Y. F. Hsu, Y. Y. Xi, K. H. Tam, A. B. Djuris'ic', J. Luo, C. C. Ling, C. K. Cheung, A. M. C. Ng, W. K. Chan, X. Deng, C. D. Beling, S. Fung, K. W. Cheah, P. W. K. Fong and C. C. Surya, *Adv. Funct. Mater.*, 2008, 18, 1020.
185. D. Li, Z. T. Liu, Y. H. Leung, A. B. Djuris'ic', M. H. Xie and W. K. Chan, *J. Phys. Chem. Solids*, 2008, 69, 616.
186. J. B. Cui and U. J. Gibson, *Appl. Phys. Lett.*, 2005, 87, 133108.
187. H. Z. Zhang, R. M. Wang and Y. W. Zhu, *J. Appl. Phys.*, 2004, 96, 624.
188. J. B. Cui, C. P. Daghljan, U. J. Gibson, R. Püsche, P. Geithner and L. Ley, *J. Appl. Phys.*, 2005, 97, 044315.
189. H. Zhang, D. Yang, X. Ma and D. Que, *J. Phys. Chem. B*, 2005, 109, 17055.
190. B. Cao, W. Cai, G. Duan, Y. Li, Q. Zhao and D. Yu, *Nanotechnology*, 2005, 16, 2567.
191. C. -H. Hung and W. -T. Whang, *J. Cryst. Growth*, 2004, 268, 242.
192. C. Ye, Y. Bando, X. Fang, G. Shen and D. Golberg, *J. Phys. Chem. C*, 2007, 111, 12673.
193. Y. Yun, G. Tailiang and J. Yadong, *J. Semicond.*, 2012, 33, 043003.
194. D. Pradhan, M. Kumar, Y. Ando and K. T. Leung, *ACS appl. mater. Interfaces*, 2009, 1, 789.
195. H. Jiang, J. Hu, F. Gu and C. Li, *Nanotechnology*, 2009, 20, 055706.
196. S. S. Warule, N. S. Chaudhari, J. D. Ambekar, B. B. Kale and M. A. More, *ACS Appl. Mater. Interfaces*, 2011, 3, 3454.
197. A. Wei, X. W. Sun, C. X. Xu, Z. L. Dong, M. B. Yu and W. Huang, *Appl. Phys. Lett.*, 2006, 88, 213102.
198. S. Maiti, U. N. Maiti and K. K. Chattopadhyay, *CrystEngComm*, 2012, 14, 8244.
199. Z. Zhang, G. Meng, Q. Xu, Y. Hu, Q. Wu and Z. Hu, *J. Phys. Chem. C*, 2010, 114, 189

200. U. N. Maiti, Sk. F. Ahmed, M. K. Mitra, K. K. Chattopadhyay, *Mater. Res. Bull.*, 2009, 44, 134.
201. U. N. Maiti, S. Nandy, S. Karan, B. Mallik, and K. K. Chattopadhyay, *Appl. Surf. Sci.*, 2008, 254, 7266.
202. J. Chen, W. Lei, W. Chai, Z. Zhang, C. Li and X. Zhang, *Solid-State Electronics*, 2008, 52, 294.
203. J. Cheng, R. Guo, and Q.-M. Wang, *Appl. Phys. Lett.*, 2004, 85, 5140.
204. H. W. Kang, J. Yeo, J. O. Hwang, S. Hong, P. Lee, S. Y. Han, J. H. Lee, Y. S. Rho, S. O. Kim, S. H. Ko and H. J. Sung, *J. Phys. Chem. C*, 2011, 115, 11435.
205. H. Hu, K. Yu, J. Zhu and Z. Zhu, *Appl. Surf. Sci.*, 2006, 252, 8410.
206. J. P. Liu, C. X. Xu, G. P. Zhu, X. Li, Y. P. Cui, Y. Yang and X. W. Sun, *J. Phys. D: Appl. Phys.*, 2007, 40, 1906.
207. S. K. Marathe, P. M. Koinkar, S. S. Ashtaputre, M. A. More, S. W. Gosavi, D. S. Joag and S. K. Kulkarni, *Nanotechnology*, 2006, 17, 1932.
208. S. Pal, S. Maiti, U. N. Maiti and K. K. Chattopadhyay, *RSC Adv.*, 2015, 5, 81176.
209. A. Dev, S. Kar, S. Chakrabarti and S. Chaudhuri, *Nanotechnology*, 2006, 17, 1533.
210. Z. H. Chen, Y. B. Tang, Y. Liu, G. D. Yuan, W. F. Zhang, J. A. Zapien, I. Bello, W. J. Zhang, C. S. Lee and S. T. Lee, *J. Appl. Phys.*, 2009, 106, 064303.
211. G. Chen, W. Wang, J. Peng, C. He, S. Deng, N. Xu and Z. Li, *Phys. Rev. B: Condens. Matter Mater. Phys.*, 2007, 76, 195412.
212. N. S. Ramgir, D. J. Late, A. B. Bhise, I. S. Mulla, M. A. More, D. S. Joag and V. K. Pillai, *Nanotechnology*, 2006, 17, 2730.
213. J. Liu, J. She, S. Deng, J. Chen and N. Xu, *J. Phys. Chem. C*, 2008, 112, 11685.
214. J.-H. Lee, Y.-W. Chung, M.-H. Hon, I.-C. Leu, *Appl. Phys. A*, 2009, 97, 403.
215. N. Liu, G. Fang, W. Zeng, H. Long, L. Yuan and X. Zhao, *Appl. Phys. Lett.*, 2009, 95, 153505.
216. G. Zhang, Q. Zhang, Y. Pei and L. Chen, *Vacuum*, 2004, 77, 53.
217. X. Liu, M. Hu, X. Chu and Q. Yan, *J. Mater. Sci.: Mater. Electron*, 2013, 24, 2839.
218. F. Ye, X.-M. Cai, F.-P. Dai, D.-P. Zhang, P. Fan and L.-J. Liu, *Phys. B*, 2012, 407, 64.
219. U. K. Gautam, L. S. Panchakarla, B. Dierre, X. Fang, Y. Bando, T. Sekiguchi, A. Govindaraj, D. Golberg and C. N. R. Rao, *Adv. Funct. Mater.*, 2009, 19, 131.
220. H. A. Rafeie, R. M. Nor, Y. M. Amin, *Mater. Express*, 2015, 5, 226.
221. R. R. Devarapalli, D. R. Shinde, F. B.-Bouaifel, S. G. Yenchalwar, R. Boukherroub, M. A. More and M. V. Shelke, *J. Mater. Chem.*, 2012, 22, 22922.

222. D. Pradhan, M. Kumar, Y. Ando and K. T. Leung, *J. Phys. Chem. C*, 2008, 112, 7093.
223. S. H. Jo, D. Banerjee and Z. F. Ren, *Appl. Phys. Lett.*, 2004, 85, 1407.
224. X. Kai, Y. X.- Hong, D. S.- Long, Y. Y.- Rong, X. Yang and G. Z.- Hui, *Chinese Phys.*, 2006, 15, 460.
225. Y. L.-min and Z. C.-chuna, *Appl. Surf. Sci.*, 2009, 255, 8359.
226. C. J. Park, D.-K. Choi, J. Yoo, G.-C. Yi and C. J. Lee, *Appl. Phys. Lett.*, 2007, 90, 083107.
227. S. C. Navale, F. J. Sheini, S. S. Patil, I. S. Mulla, D. S. Joag, M. A. More and S. W. Gosavi, *J. Nano Res.*, 2009, 5, 231.
228. Q. Zhao, X. Y. Xu, X. F. Song, X. Z. Zhang, D. P. Yu, C. P. Li and L. Guo, *Appl. Phys. Lett.*, 2006, 88, 033102.
229. S. M. Gupta and M. Tripathi, *Chinese Sci Bul.*, 2011, 56, 1639.
230. A. Hagfeldt and M. Grätzel, *Chem. Rev.*, 1995, 95, 49.
231. D. Mijin, M. Savić, P. Snežana, A. Smiljanić, O. Glavaški, M. Jovanović and S. Petrović, *Desalination*, 2009, 249, 286.
232. N. Daneshvar, D. Salari and A. R. Khataee, *J. Photochem. Photobiol., A*, 2004, 162, 317.
233. S. Chakrabarti and B. K. Dutta, *J. Hazard. Mater. B*, 2004, 112, 269.
234. R. Ullah and J. Dutta, *J. Hazard. Mater.*, 2008, 156, 194.
235. S. Sakthivel, B. Neppolian, M. V. Shankar, B. Arabindoo, M. Palanichamy and V. Murugesan, *Sol. Energy Mater. Sol. Cells*, 2003, 77, 65.
236. C. A. K. Gouvea, F. Wypych, S. G. Moraes, N. D. N. Nagata and P. P. -Zamora, *Chemosphere*, 2000, 40, 433.
237. S. K. Kansal, M. Singh and D. Sud, *J. Hazard. Mater.*, 2007, 141, 581.
238. R. Comparelli, E. Fanizza, M. L. Curri, P. D. Cozzoli, G. Mascolo and A. Agostiano, *Appl. Catal., B*, 2005, 60, 1.
239. M. L. Curri, R. Comparelli, P. D. Cozzoli, G. Mascolo and A. Agostiano, *Mater. Sci. Eng. C*, 2003, 23, 285.
240. M. A. Behnajady, N. Modirshahla and R. Hamzavi, *J. Hazard. Mater. B*, 2006, 133, 226.
241. C. Ye, Y. Bando, G. Shen, and D. Golberg, *J. Phys. Chem. B*, 2006, 110, 15146.
242. D. Drijvers, H. V. Langenhove and M. Beckers, *Water Res.*, 1999, 33, 1187.
243. C. Richard and P. Boule, *J. Photochem Photobiol A: Chem*, 1994, 84, 152.

244. J. Domenech and J. Peral, *Sol. Energy*, 1988, 41, 55.
245. L. B Khalil, W. E Mourad and M. W. Rophael, *Appl. Catal., B*, 1998, 17, 267.
246. A. A. Khodja T. Sehili, J. -F. Pilichowski and P. Boule, *J. Photochem. Photobiol., A*, 2001, 141, 231.
247. Y. Tong, J. Cheng, Y. Liu and G. G. Siu, *Scr. Mater.*, 2009, 60, 1093.
248. B. Jia, W. Jia, F. Qu and X. Wu, *RSC Adv.*, 2013, 3, 12140.
249. N. M. Flores, U. Pal, R. Galeazzi and Alberto Sandoval, *RSC Adv.*, 2014, 4, 41099.
250. H. K. Egzar, M. S. Mashkour and A. M. Juda, *Int. J. Eng. Technol. IJET –IJENS*, 2013, 13, 26.
251. A. Akyol, H.C. Yatmaz and M. Bayramoglu, *Appl. Catal., B*, 2004, 54, 19.
252. T. Zhai, S. Xie, Y. Zhao, X. Sun, X. Lu, M. Yu, M. Xu, F. Xiao and Yexiang Tong, *CrystEngComm*, 2012, 14, 1850.
253. H. Sun, Y. Yu, J. Luo, M. Ahmad and J. Zhu, *CrystEngComm*, 2012, 14, 8626.
254. G. R. Li, T. Hu, G. L. Pan, T. Y. Yan, X. P. Gao and H. Y. Zhu, *J. Phys. Chem. C*, 2008, 112, 11859.
255. E. S. Jang, J. -H. Won, S. -J. Hwang and J. -H. Choy, *Adv. Mater.*, 2006, 18, 3309.
256. Y. Wang, X. Li, G. Lu, X. Quan and G. Chen, *J. Phys. Chem. C*, 2008, 112, 7332.
257. X. Zhang, J. Qin, Y. Xue, P. Yu, B. Zhang, L. Wang and R. Liu, *Sci. Rep.*, 2014, 4, 4596
258. Y. Zheng, C. Chen, Y. Zhan, X. Lin, Q. Zheng, K. Wei, J. Zhu and Y. Zhu, *Inorg. Chem.*, 2007, 46, 6675.
259. J. Wang, P. Liu, X. Fu, Z. Li, W. Han and X Wang, *Langmuir*, 2009, 25, 1218.
260. S. Khezrianjoo and H. D. Revanasiddappa, *Chem. Sci. J.*, 2012, 2012, CSJ-85.
261. L. A. Ghule, A. A. Patil, K. B. Sapnar, S. D. Dhole and K. M. Garadkar, *Toxicol. Environ. Chem.*, 2011, 93, 623.
262. H. Wang, C. Xie, W. Zhang, S. Cai, Z. Yang and Y. Gui, *J. Hazard. Mater.*, 2007, 141, 645.
263. K. Byrappa, A. K. Subramani, S. Ananda, K. M. L. Rai, R. Dinesh and M. Yoshimura, *Bull. Mater. Sci.*, 2006, 29, 433.
264. D. H. Mohsin, A. M. Juda, M. S. Mashkour, *Int. J. Eng. Technol.*, 2013, 13, 34.
265. B. Zielinska, J. Grzechulska, R. J. Kalenczuk and A. W. Morawski, *Appl. Catal., B*, 2003, 45, 293.
266. E. Evgenidou, K. Fytianos and I. Poullos, *Appl. Catal., B*, 2005, 59, 81.

267. S. R. Kanel and S. R. A.-Abed, *J. Nanopart. Res.*, 2011, 13, 4035.
268. A. Akyol and M. Bayramoglu, *J. Hazard. Mater. B*, 2005, 124, 241.
269. L.-Y. Fan and S.-H. Yu, *Phys. Chem. Chem. Phys.*, 2009, 11, 3710.
270. C. Yu, K. Yang, Y. Xie, Q. Fan, J. C. Yu, Q. Shua and C. Wang, *Nanoscale*, 2013, 5, 2142.
271. T. Xu, L. Zhang, H. Cheng and Y. Zhu, *Appl. Catal., B*, 2011, 101, 382.

Table 1. Summary of methods of obtaining zinc oxide

Dim	Method	Precursors	Synthesis conditions	Morphology / Properties/ Applications	Ref
0-D	Precipitation process	Zn(NO ₃) ₂ , NaOH	2 h; drying: 2 h, 100°C	Spherical sized particles	30
		Zinc acetate, and KOH	20–80°C; drying: 120°C	Particles diameter: 160–500 nm	120
	Solution processed	Ethanol, Zn(CH ₃ CO ₂) ₂ , 2H ₂ O, NaOH	Stirring 30 min 40°C, Centrifugation, drying	Wurtzite structure, nanocrystals crystal size :10 nm, PL, EL emission	121
		Zinc acetate, NaOH, hexamethylenetetraamine	5–10 h, 100–200°C; HMTA: 0–200 ppm	Spherical shape; particles diameter: 55–110 nm	24
	Solvothermal, Hydrothermal and Microwave techniques	ZnCl ₂ , NaOH	5–10 h, 100–220°C	Bullet-like rod-like Particles	40
		Zinc acetate, zinc nitrate, LiOH, KOH, NH ₄ OH	Reaction: 10–48 h, 120–250°C	Hexagonal (wurtzite) structure, Microcrystallites size: 100 nm–20 μm	122
		Zinc acetate, NH ₃ , TMAH, zinc 2-ethylhexanoate, 2-propanol	15 min, 2–72 h; final pH: 7–10	Particles with irregular ends and holes; aggregates with particles of 20–60 nm	25
		Trimethylamine N-oxide, EDA, 4-picoline N-oxide, HCl, toluene, N,N,N',N'-TMEDA	Reaction: 24–100 h, 180°C	Wurtzite structure; particles morphology: nanoparticles (24–60 nm)	47
		Zn(NO ₃) ₂ , HMTA	Microwave heating: 2 min, 90°C	Nanorod and nanowire shape, electronic and optoelectronic devices	123
		Zinc acetylacetonate, methoxyethoxy, n-butoxyethanol, zinc oximate	Microwave heating: 800 W, 4 min	Zincite structure; average crystallite size: 9–31 nm, particles diameter: 40–200 nm; BET: 10–70 m ² /g	44
1-D	chemical bath deposition (CBD)	Zinc acetate, NaOH, zinc nitrate diethylenetriamine, Methanol	Reaction: 90–95°C for 60 min	Nanorods, room-temperature photoluminescence	124
		Zinc nitrate and HMTA	above 90°C	Open and closed hexagonal nanorods	125
	Methanolic solution, zinc acetate, cadmium acetate, N, N, N', N'-tetramethylethylenediamine	Zinc nitrate, methenamine	5 h, 12 h, 28 h at 90 °C	Nanorods, photoluminescence	126
		Methanolic solution, zinc acetate, cadmium acetate, N, N, N', N'-tetramethylethylenediamine	annealed at 150°C for 5 min, deposition 70°C without stirring for 2-4 h	Hexagonal shape: nanorod arrays, colloidal lithography	125
	Electrochemical	Ammonia hydroxide	7 h, 80 °C	Hexagonal dots	127
		Ag/AgCl electrode, Zn(NO ₃) ₂	Electrochemical deposition: 65°C	Rod Arrays, photoluminescence property and field emission application	128

Electrodeposition (aqueous)	electrolyte bath containing 0.05 M $Zn(NO_3)_2$ and 0.1 M NaF	55 and 60 °C at -1.1 V	Rhombus-shaped ZnO nanorod arrays, improved hydrogen storage capacity	129
Low temperature, Solvothermal, Hydrothermal and Microwave techniques	Zinc nitrate hexahydrate, methenamine and PVA Si substrate, SiO_2 , zinc nitrate hexahydrate, diethylenetriamine Zinc nitrate, HMTA Zinc nitrate, NaOH, ethylenediamine Zinc foil, acetone, ethanol, NaOH	Reaction: 95 °C for 8 h PECVD, rf sputtering, 75 °C, 30 min 370K for 10 h Reaction: 180 °C for 20 h 170–230 °C, 3–12 h	Wurtzite structured nanorod array, high transmittance, optical transmittance Nanowire triode, field emission, 50 nm diameter, $3.4 \times 10^{10} \text{ cm}^{-2}$ number density Pure wurtzite type nanorods Free-standing ZnO nanorod, diameter and length are 45.6 nm and 1.54 μm Nanorod Arrays, photoluminescence	130 131 132 133 64
Precipitation process	zinc acetate, NH_3 aq. ZnO powder, NH_4HCO_3 $Zn(NO_3)_2$, NaOH, SDS, TEA	85 °C; drying: 10 h, 60 °C Reaction: 2 h, 25 °C 50–55 min, 101 °C	Rods, flower-like particles Hexagonal wurtzite rod-like shape Nut-like and rice-like rod	134 135 136
Solution Processed	Zinc acetate, methanol, KOH, chloroform, n-butylamine $Zn(NO_3)_2$, HMTA	Stirring, condensed and heated for 5 h Sonicate at 50 °C for 30 min, immersed in 95 °C water bath for 4 h	Nanorods(65-nm-long, 10-nm-wide), thin-film transistors (TFTs) Aligned ZnO nanorod, average diameter ~ 100 nm and average length ~500 nm	137 138
Solvothermal Route	NaOH or HCl, ethanol, Zinc nitrate hexahydrate	Reaction: 200 °C for 12 h	Single crystalline hexagonal cross-section, nano/micro columns and cones	139
Wet chemical room temperature	Ammonium persulphate, NaOH, zinc metal powder Sodium peroxide, Zn foil Methylbenzene, acetone, ethanol, HF solution, zinc acetate, hexamethylenetetramine	Reaction: Room temperature, 20 h At room temperature, 2h CBD technique used on seed layer: 65 °C to 95 °C	Nanowires (length 300- 500 nm, diameter 15 nm), UV catalyst ZnO nanorod (5 nm diameter) arrays Hexagonal wurtzite, nanorod arrays, photoluminescence property	140 141 142
Other method	$Zn(NO_3)_2$, hexamethylenetetramine	Ultrasonic irradiation: 30 min, 80 °C	Nanorod and nanowire shape, electronic and optoelectronic devices	123
Precipitation	$ZnSO_4$, NH_4OH , NH_4HCO_3	30 min, 60 °C	Hexagonal structure, flake-like	143
Room temperature soft chemical route	Chromic acid, detergent	Stirring kept at room	Nanofibrous wurtzite ZnO thin film, orthorhombic crystal structure, optical, electrical, LPG sensing properties	144

3-D	Other method	Zn(NH ₃) ₄ ²⁺ , ammonia, zinc acetate dihydrate, distilled water	Reaction: 85 °C for 10 h	Flower-like ZnO nano/microstructures, photoluminescence	145
	Chemical precipitation	Milli-Q ultrapure water, NaOH, Zn(NO ₃) ₂	Aging: room temperature, pH- 9 and 12 h	Snowflake like structures, ozone decomposition in water	146
	Solution deposition method	Trimethylgallium , NH ₄ OH Trimethylindium, NH ₃ ,zinc acetate, polytetrafluoroethylene,	Reaction: at 100°C for 2 h	Nanorods and nanoflowers (nanoflowers were synthesized on the nanorods)	147
	Solvothermal method	Zn(NO ₃) ₂ , NaOH, ethanol, anhydrous ethanol	Reaction: 190°C for 12 h	Nanoflowers assembled by many thin and uniform nanosheets	148
	Hydrothermal method	NaOH, N ₂ H ₄ ·H ₂ O	Reaction: at 90°C for 5 h	Rod-like and chrysanthemum-like ZnO nanostructures, photo-catalysts	149
		Zinc nitrate, CTAB and HMTA	Reaction: 80-90°C, 0.5-6h	ZnO nanoflowers, single crystal	151
		Zn(NO ₃) ₂ , NaOH, CTAB	temperature range 120–220°C, 30 min	ZnO nanostructure with sisal-like morphology	152
		Zn(NO ₃) ₂ , ammonium hydroxide	pH: 11.30, 70°C, 12h, again pH: 10.8, 70°C, 6 h	Flower like microstructure and nanorod array, Dye-sensitized solar cell	153
	Precipitation process	Zn(NO ₃) ₂ , NH ₄ HCO ₃ Zinc acetate, NaOH	2 h, 25°C; drying: 80°C Reaction: 30 min, 75 °C	Flower-like shape Flower shape, antimicrobial activity	135 150
	Other method	Zn(NH ₃) ₄ ²⁺ , ammonia, zinc acetate dihydrate, distilled water	Reaction: 85 °C for 10 h	Flower-like ZnO nano/microstructures, photoluminescence	145

Table 2: Field emission parameters of the reported ZnO nanostructures We define the turn-on and threshold field at a field producing emission current density of 10 μ A/cm² and 1mA/cm² respectively. If other values are used, this is mentioned separately.

ZnO emitter	Synthesis method	Turn-on field (V/ μ m)	Threshold field (V/ μ m)	Field enhancement factor (β)	Ref
Nanorod	Aqueous chemical route	4.6	9.5	2923	198
Hierarchical nanosheet	Chemical Reaction	3.5	7.3	4026	198
Nanorod Array	Electrochemical deposition (ECD)	2	5	1680	189
Nanowires		15.5 and 9.5 (0.1 μ A/cm ²)	18 (<250 μ A/cm ²)	1188 and 1334	109
Nanosheet on ITO		3.6 (0.1 μ A/cm ²)	-	4700	91

Nanowire	9.5	-	1334	196
Nanoneedle arrays	22.1	-	-	190
Nanopillars and nanoflowers	0.16 and 0.24	0.36 and 0.42	1802 and 397	193
Aligned Nanorods	7.87		1429.70	199
Nanospikes and Nanopillars	3.2, 6.2	6.6,-	2364, 1170	194
ZnO nanoneedles	3.6	4.4	2664	200
Nanotubes	7 (0.1 $\mu\text{A}/\text{cm}^2$)	17.8	910	197
3D urchin-like nanostructure	3.7	4.8	1239	195
Nanoneedles	4.2	7.2	2350	42
Nanopencils	7.5	11.3	1140	42
Nanorod	3.2	7.8	5400	201
Nanorod	1.9 (0.2 $\mu\text{A}/\text{cm}^2$)	7.4	2510	202
Tubular microrods	5.6 (1 $\mu\text{A}/\text{cm}^2$)	20.2 (11 mA/cm^2)	-	203
Needleleaf-like nanowire array	2.01	-	-	204
Nanowire square patterned array	1.60	-	1202	204
Nanonunchakus	3.0	5.47	1592	205
Nanoneedles	3.0	19.0	8504	206
Nanorods with Pt/Ag nanoparticles	1.9	-	-	192
nanoneedles	2.3	4.2 (<75 $\mu\text{A}/\text{cm}^2$)	2080	207
nanorods	2.5	5.0 (<75 $\mu\text{A}/\text{cm}^2$)	2040	207
nanowire arrays	7.1 (10 $\mu\text{A}/\text{cm}^2$)	13.0 (10 mA/cm^2)	862	207
Nanowires	1.6 (1 $\mu\text{A}/\text{cm}^2$)	2.1	3340	131
Nanotip arrays	10.8 (0.1 $\mu\text{A}/\text{cm}^2$)	19.5	590	191
Nanospike	3.01	-	4473	208
Nanocactus	1.44	4.10	14619	208
Nanotree	2.03	5.09	8771	208
Pin-cushion cactus like nano-pencil film	1.38 (0.1 $\mu\text{A}/\text{cm}^2$)	2.84 (49 $\mu\text{A}/\text{cm}^2$)	-	196
Nanorods	5.3	-	850 – 1044	209

Table 3: Chemical structures of the dyes employed in ZnO-assisted photocatalysis

Class	Dye/ λ_{max} (nm)	Chemical structure	Molecular formula	Class	Dye/ λ_{max} (nm)	Chemical structure	Molecular formula
Azo	Methyl Red (410 nm)		$\text{C}_{15}\text{H}_{15}\text{N}_3\text{O}_2$	Xanthene	Rhodamine 6G (524 nm)		$\text{C}_{28}\text{H}_{31}\text{N}_2\text{O}_3\text{Cl}$
	Methyl Orange (410 nm)		$\text{C}_{14}\text{H}_{14}\text{N}_3\text{NaO}_3\text{S}$		Rhodamine (Rh B) (551 nm)		$\text{C}_{28}\text{H}_{31}\text{ClN}_2\text{O}_3$
	Congo red (450nm)		$\text{C}_{32}\text{H}_{22}\text{N}_6\text{Na}_2\text{O}_6\text{S}_2$		Eosin (514 nm)		$\text{C}_{20}\text{H}_8\text{Br}_2\text{N}_2\text{O}_9$
	Metanil Yellow (536nm)		$\text{C}_{18}\text{H}_{14}\text{N}_3\text{NaO}_3\text{S}$		Rose Bengal (550 nm)		$\text{C}_{20}\text{H}_4\text{Cl}_4\text{I}_4\text{O}_5$
	acid red 14 (515 nm)		$\text{C}_{20}\text{H}_{12}\text{N}_2\text{Na}_2\text{O}_7\text{S}_2$		Erythrosin (530 nm)		$\text{C}_{20}\text{H}_{16}\text{I}_4\text{Na}_2\text{O}_5$
Azo reactive textile dye	Remazol Red F3B (365 nm)		$\text{C}_{29}\text{H}_{19}\text{N}_3\text{Na}_4\text{O}_{17}\text{S}_5$	Phenazines	Neutral red (NR) (534 nm)		$\text{C}_{15}\text{H}_{17}\text{ClN}_4$
	Remazol Red RR (525 nm)		$\text{C}_{27}\text{H}_{18}\text{ClN}_7\text{Na}_4\text{O}_16\text{S}_5$		Thiazines	Methylene blue (MB) (665 nm)	
Nitro	C.I. Acid Yellow23 (428 nm)		$\text{C}_{16}\text{H}_9\text{N}_4\text{Na}_3\text{O}_9\text{S}_2$		Methylene blue (650 nm)		$\text{C}_{18}\text{H}_{22}\text{N}_3\text{S}_2\text{Cl}$ ZnCl_2

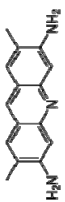
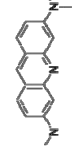
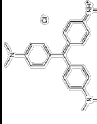
Acridines	Acridine yellow (442 nm)		$C_{15}H_{15}N_3$	Thionine (TH ⁺) (596 nm)	$C_{12}H_{10}N_3S$
Acridines	Acridine orange (492 nm)		$C_{17}H_{19}N_3$	Azure B (647 nm)	$C_{15}H_{16}ClN_3S$
Triphenyl methane derivative	Methyl violet (580 nm)		$C_{24}H_{28}N_3Cl$	Triarylm ethane	$C_{23}H_{25}ClN_2$

Table 4. Photocatalytic degradation of various compounds by ZnO nanoforms

Target compound	Comments on photocatalytic performance	Ref
Organic dye- Methylene Blue	Increase of catalyst loading increases the photodegradation from 58 to 76% in 2 h	216
Organic dye- Eosin	Increase of catalyst loading increases the photodegradation from 47 to 74% in 2 h	216
Textile dye- Acid red 14 AR14)	The complete removal of color could be achieved in a relatively short time of about 1 h	215
Aniline dye- Methylene Blue	50% of MB degraded within 10 min by ZnO	217
Complex diazo dye- Acid Brown 14	Completely colourless within 120 min. Complete mineralisation was attained with the formation of carbon dioxide, water, nitrate, ammonia, sulphate and chloride.	218
Remazol Brilliant Blue R, Reactive Blue 221	Decolorization of dyes in reaction times of 60 min. Extending the photochemical treatment up to 120 min, mineralization higher than 80% for all the dyes was observed.	219
Methyl Orange, Rhodamine 6G	The maximum adsorption of MO was noticed at pH 4 and of R6G at pH 10	220
Methyl Red and Methyl Orange	surfactant-capped nanocrystals exhibit more versatile performance than conventional catalyst	221
Organic dye- Methyl Red	High photocatalytic efficiency of nanosized semiconducting particles.	222
Azo dye- C.I. Acid Yellow 23	Adsorption constant K_{ads} and rate constant k_{L-H} increases with increasing light intensity	223
Organic dyes- Eosin B, Methyl Orange, and Methyl Red	Eosin B disappears almost completely after ~30 min; photodegradation time of methyl orange and methyl red of ~60 and ~75 min, respectively	224
Phenol and Trichloroethylene	Oxidant: H ₂ O ₂ . Reaction temperature (°C): 29.5 °C	225
Salicylic acid	Intermediates detected: 2,5- DHBA, pyrocatechol	226
Potassium Cyanide	It a good catalyst even in the case of solar irradiation CN ⁻ gives OCN ⁻ as intermediate	227
Cr(VI)	Reduction of Cr(VI) to Cr(III)	228
2-phenylphenol	2-phenylphenol (OPP) can be photocatalytically degraded on ZnO efficiently	229
Malachite Green (MG)	ZnO flowers exhibited highest photocatalytic activity due to highest surface oxygen vacancy	230

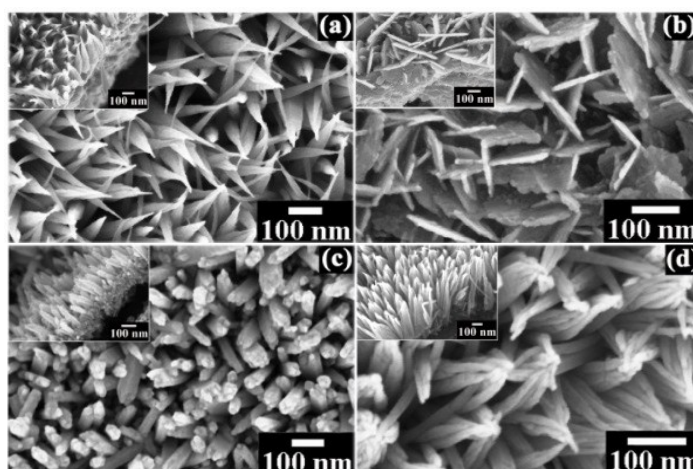


Figure 1: FESEM images of ZnO morphological assortment via zinc counter ion variation [36] Reproduced with permission Copyright Royal Society of Chemistry.

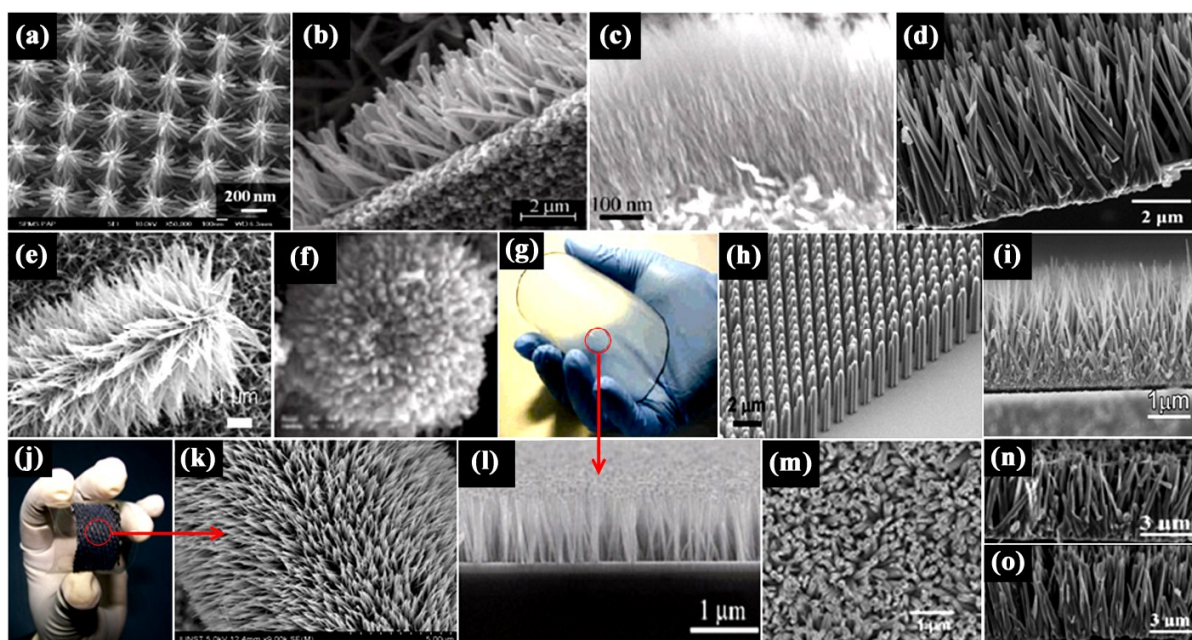


Figure 2: FESEM images of ZnO nanowire arrays grown on ZnO seeded substrates; (a) Si substrate [49], (b) thin film [45], (c) Zn substrate [55], (d,n,o) alloy, Ti, Ni substrate [38], (e) FTO substrate [51], (f) polystyrene microsphere [52], (h) GaN substrate [54], (g,l) TPU flexible substrate [53], (i) TCO substrate [55], (j,k) carbon cloth [56], (m) PET/ITO substrate [57]. Reproduced with permission (a,d,e,g,h,l,n,o) Copyright American Chemical Society (b,c) Copyright John Wiley and Sons, (f, i) Copyright Elsevier, (j, k) Copyright IOP Publishing, (m) Copyright AIP Publishing LLC.

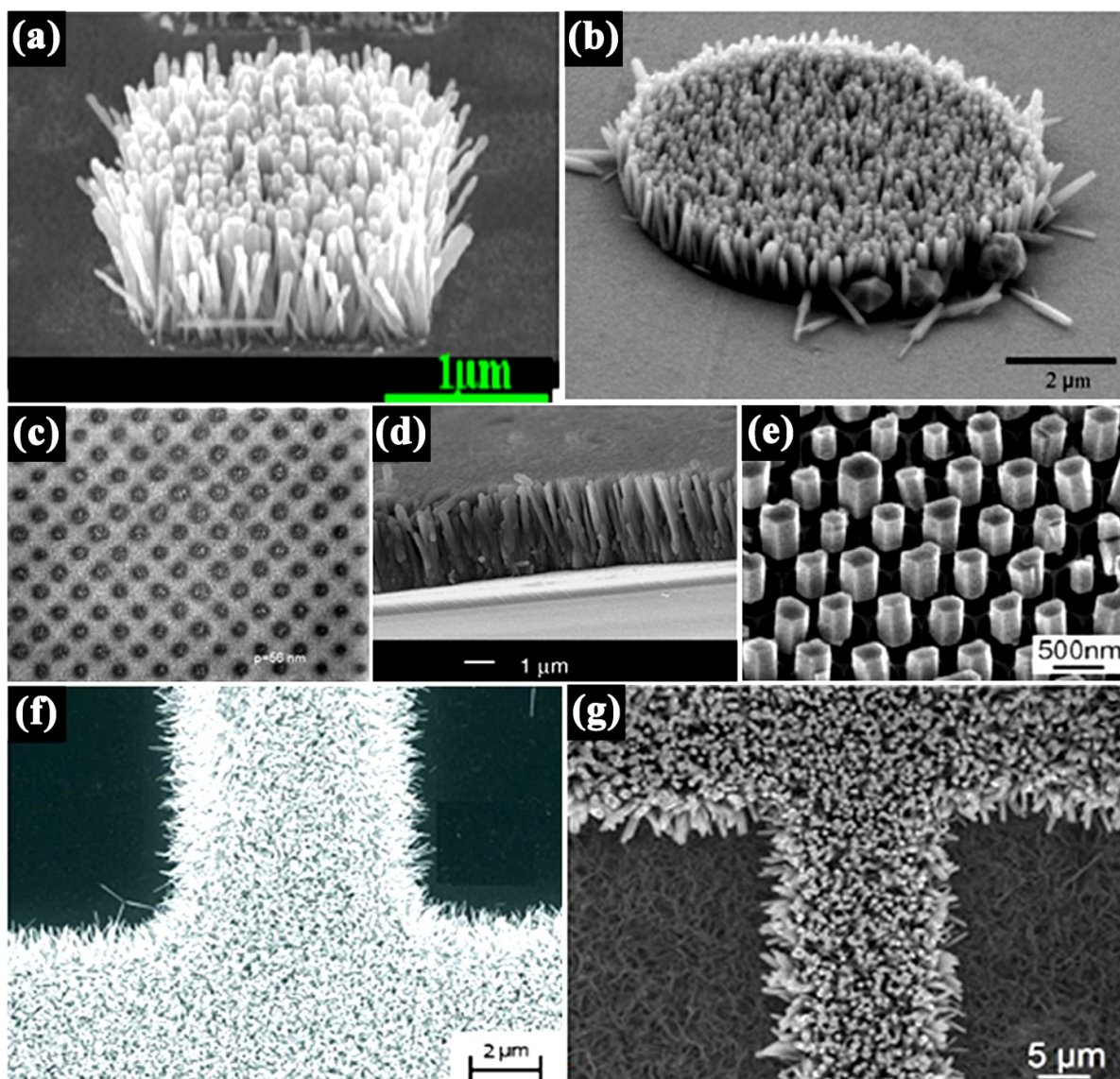


Figure 3: FESEM images of ZnO nanostructured patterned growth arrays [64-67,69,70]. Reproduced with permission (a) Copyright IOP Publishing, (b,e) Copyright American Chemical Society, (c,d) Copyright Elsevier, (f) Copyright AIP Publishing LLC, (g) Copyright Nature Publishing Group.

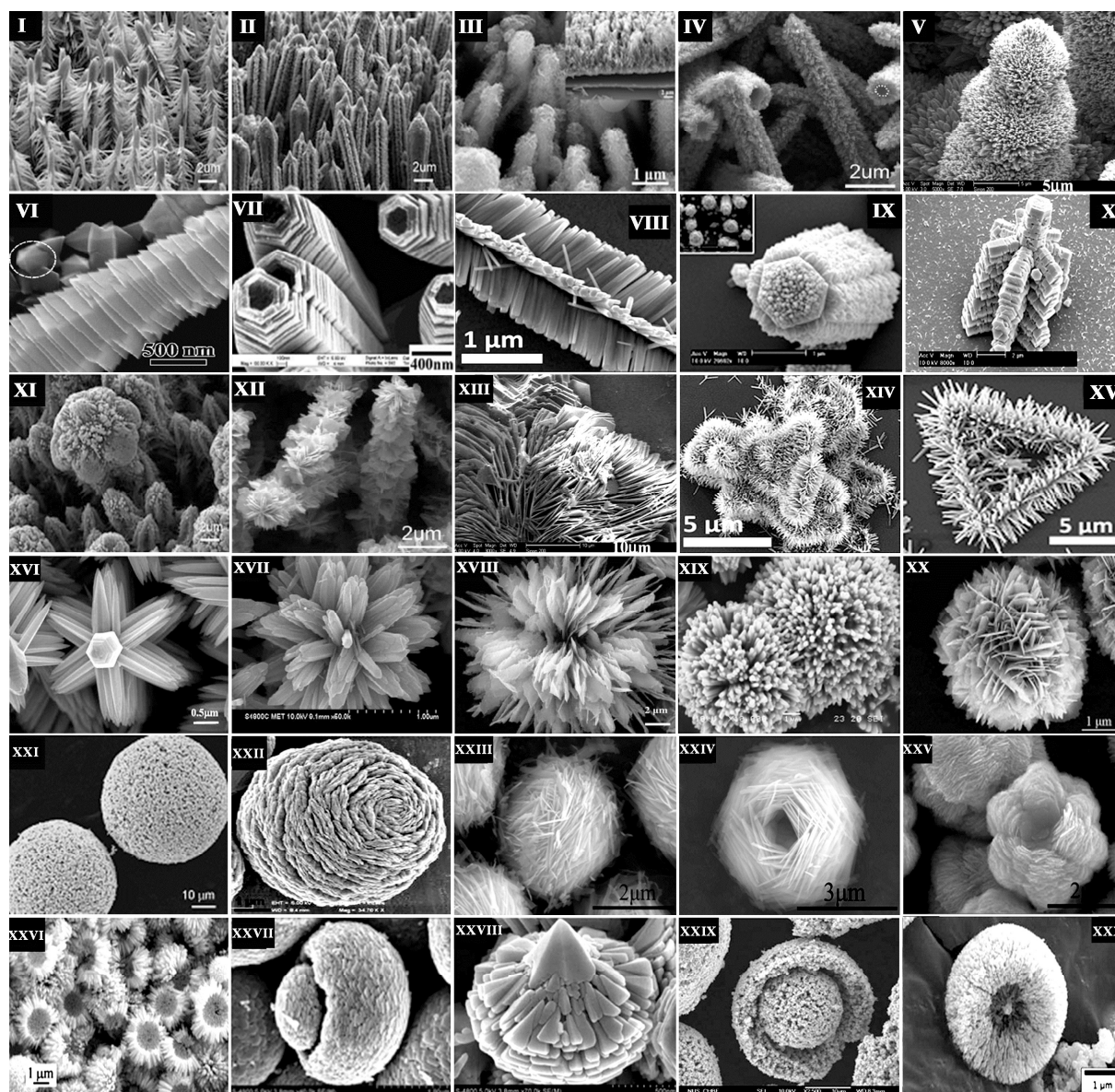


Figure 4: Collection of ZnO hierarchical and higher-dimensional nanostructures prepared via low temperature solution processed method. [81,90,96,100,102-115].

Reproduced with permission (I-IV,VIII,XI,XII,XIV,XV,XX,XXII,XXVII) Copyright Royal Society of Chemistry, (V-VII,IX,X,XIII,XVI,XVIII,XXI,XXIII-XXV,XXIX) Copyright American Chemical Society, (XXVI) Copyright John Wiley and Sons, (XVII,XIX,XXX) Copyright Elsevier.

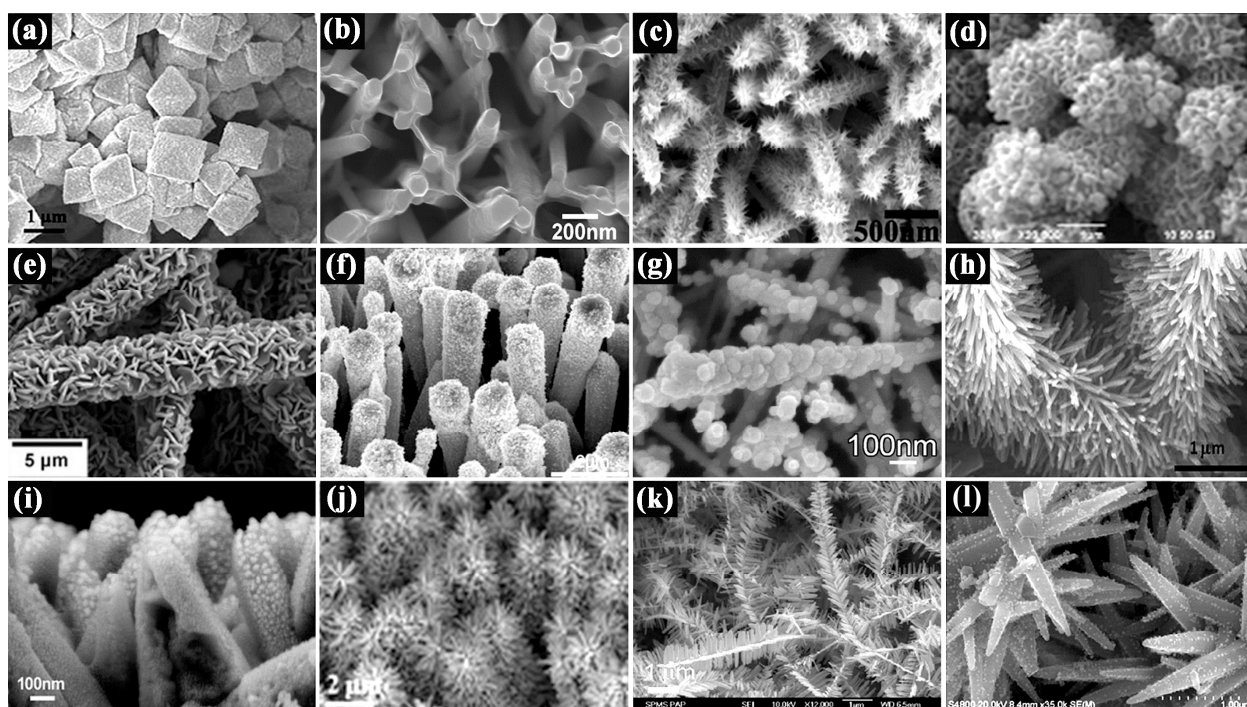


Figure 5: Few ZnO based heterostructure assemblies; [55,150-160].

Reproduced with permission (a,c-e,h-j,l) Copyright Royal Society of Chemistry, (b) Copyright IOP Publishing, (f,g,j) Copyright American Chemical Society.

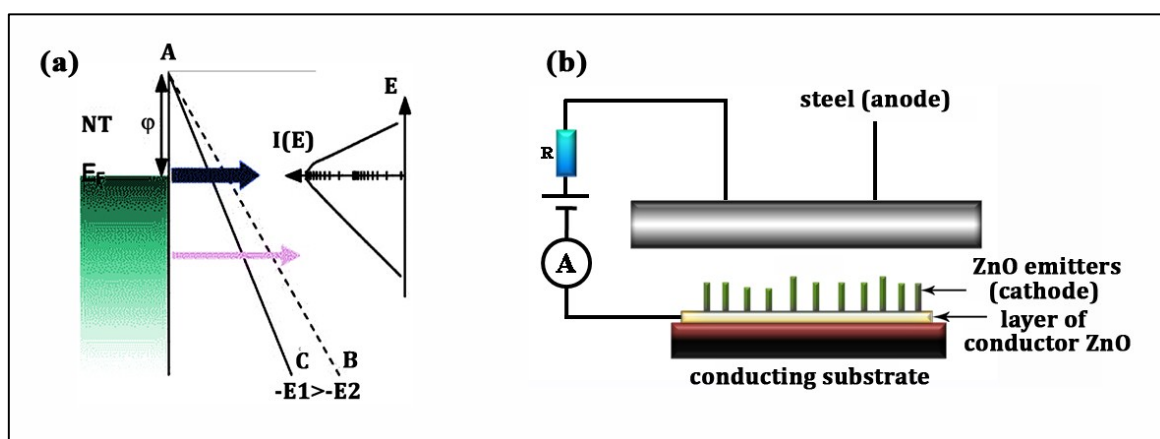


Figure 6: (a) Field emission mechanism and, (b) Schematic of field emission set up.

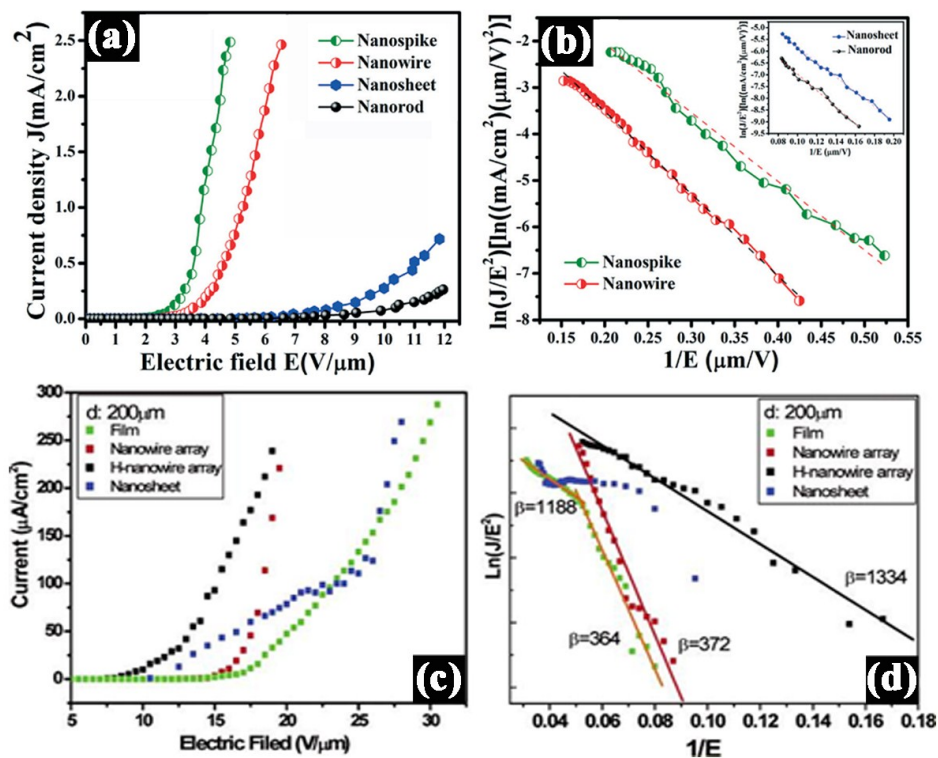


Figure 7: Variation in FE characteristics and corresponding FN plots due to the variation in emitter geometry [36, 105]. Reproduced with permission (a,b) Copyright Royal Society of Chemistry, (c,d) Copyright American Chemical Society.

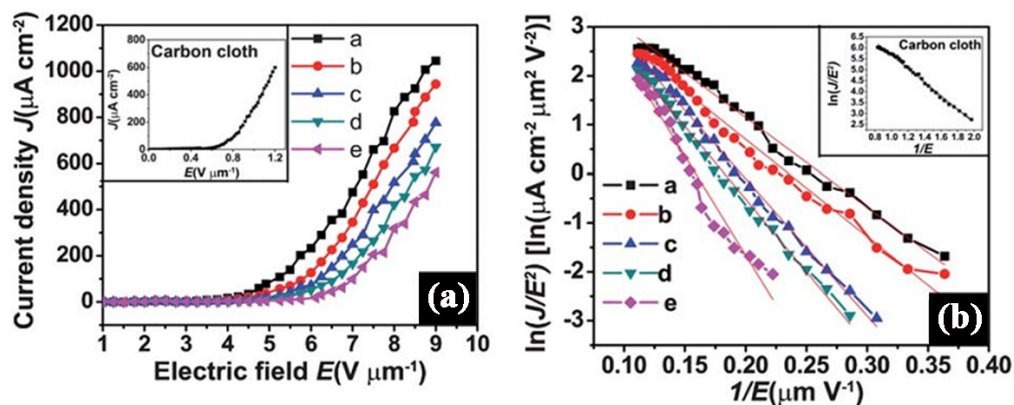


Figure 8: (A) J vs. E and F-N plot for the nanopikes over (a) ITO (b) Si (c) Ac-ITO (d) Ac-Si (e) Ac-Cu. Inset gives same plots for the nanopikes over Ac-carbon cloth. Reproduced with permission Copyright Royal Society of Chemistry.

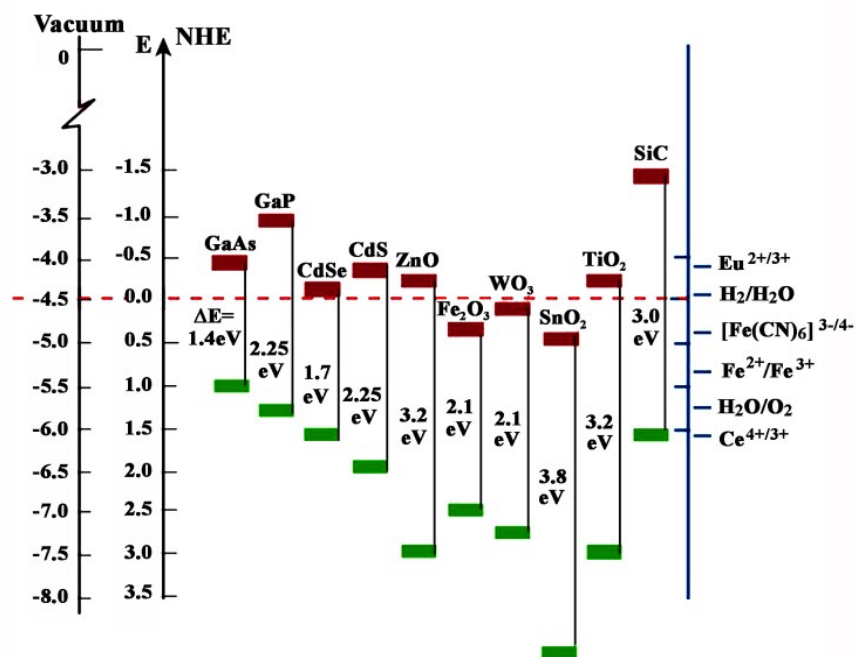


Figure 9: Band positions of several semiconductors in contact with an aqueous electrolyte at pH 1 [213].

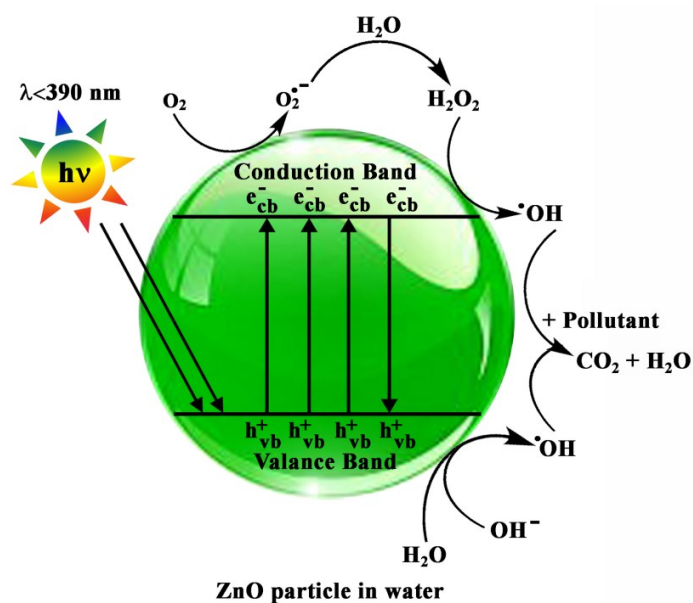


Figure 10: Basic mechanism of the photocatalysis.

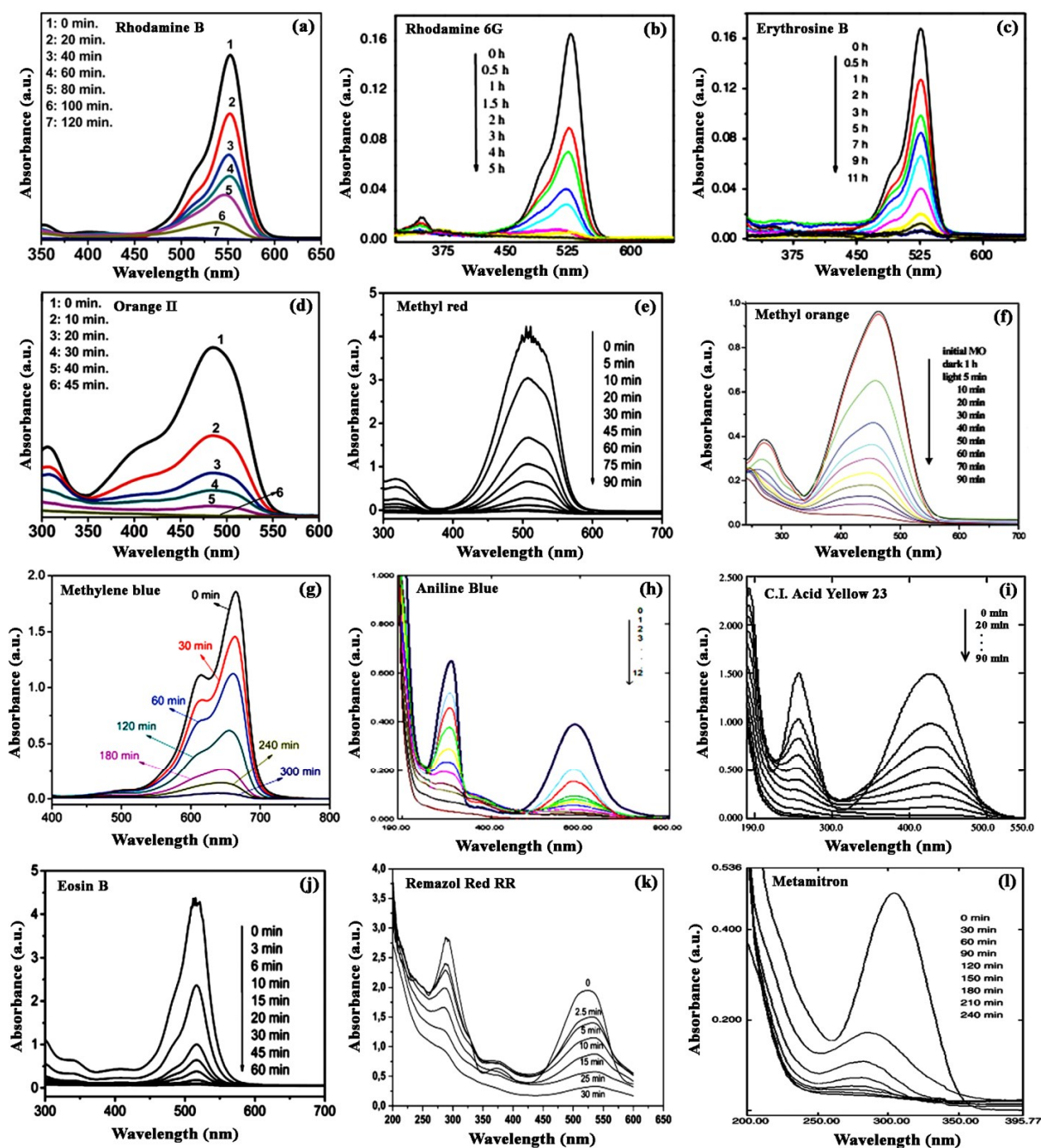


Figure 11: Temporal evolution of UV-vis absorption spectra related to different hazardous dyes. [136,214,224,226,230-234]

Reproduced with permission Copyright Royal Society of Chemistry (a,d,g,f) Copyright Elsevier (b,c,i,k,l) Copyright American Chemical Society (e,j) Copyright International Journals of Engineering & Sciences (h)

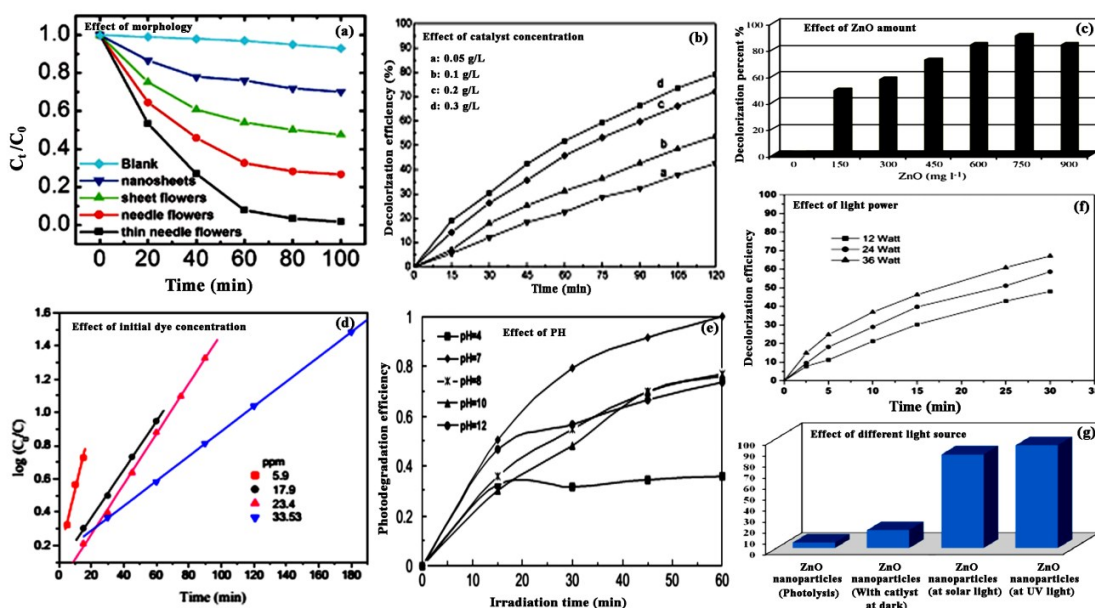


Figure 12: (a) Photocatalytic degradation curves (C_t/C_0 vs. t) of RhB in the presence of different photocatalysts; (b,c) Results showing the Effect of catalyst loading; (d) initial dye concentration; (e) pH of the solution and light sources on photocatalytic efficiency [108,215,223,234,236,245, 246].

Reproduced with permission (a) Copyright Royal Society of Chemistry, (b,c,f,g) Copyright Elsevier, (h) Copyright International Journals of Engineering & Sciences, (d) Copyright Indian Academy of Sciences.

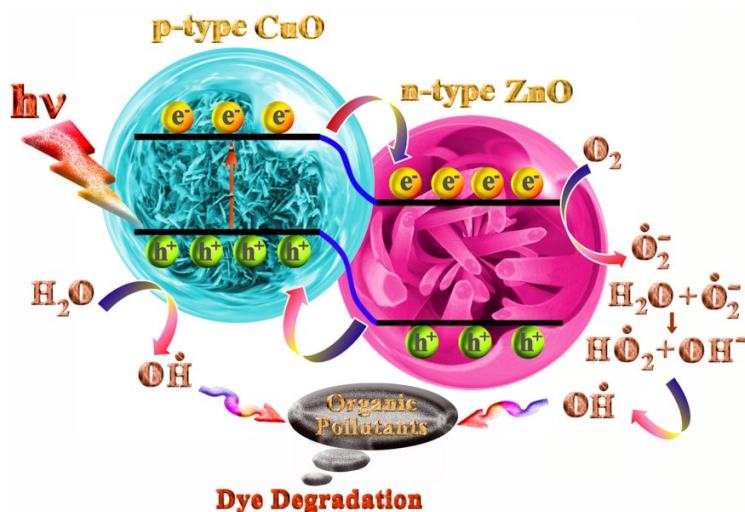


Figure 13: Schematic of photocatalytic Mechanism of ZnO/CuO heterojunction [152].

Reproduced with permission Copyright Royal Society of Chemistry.

Biography



Mr. Soumen Maiti has received his B.Sc. degree in physics from Calcutta University and then pursued his M.Sc. in applied physics from Bengal Engineering and Science University. Currently he has been working as senior research fellow under the supervision of Prof. Kalyan Kumar Chattopadhyay. His research interests include novel synthesis and applications of graphene, metal oxide and organic charge transfer complex nanostructures.



Ms. Shreyasi Pal (born 1989) obtained her B.Sc. (Hons) in Physics from Lady Brabourne College, C.U. in 2010. Later she obtained her M.Sc. in Physics from Calcutta University, Rajabajar Science College in 2012. She has been awarded “CSIR Fellowship” from HRDG, Government of India for academic year 2012–2017. She is now continuing her research as a “Senior Research Fellow of CSIR” at “Jadavpur University”. Her research interests include synthesis and applications of different metal oxides and organic charge transfer complex nanostructures, heterostructures, core–shell nanomaterials and graphene.



Dr. K.K. Chattopadhyay is an Associate Professor at the Department of Physics, and also the Director of the School of Materials Science and Nanotechnology, Jadavpur University, Kolkata. He has guided so far 24 students for Ph.D. degree and published more than 245 research papers in various international journals of repute, 4 books and a number of book chapters. His current research interests include metal oxide nanostructures, carbon nanomaterials, DFT, and p-type transparent conducting oxides and devices. He has been awarded MRSI medal from Materials Research Society, India and Dr. Meghnad Saha Gold Medal from Asiatic Society, India.